Title: Involvement of an IgE/Mast cell/B cell amplification loop in abdominal aortic aneurysm progression

Authors: Alexia Loste, PhD, [a,b], Marc Clément, PhD, [a,b], Sandrine Delbosc, PhD, [a,b], Kevin Guedj, PhD, [a,b], Jean Sénémaud, MD, [a,b,c], Anh-Thu Gaston, BS, [a,b], Marion Morvan, BS, [a,b], Guillaume Even, BS, [a,b], Grégory Gautier, PhD, [b,d], Alexander Eggel, PhD, [e], Michel Arock, PharmD, PhD, [f], Emanuele Procopio, MS, [a,b], Catherine Deschildre, BS, [a,b], Liliane Louedec, BS, [a,b], Jean-Baptiste Michel, MD, PhD [a,b], Lydia Deschamps, MD, PhD [g], Yves Castier, MD, PhD, [c], Raphaël Coscas, MD, PhD, [a,h], Jean-Marc Alsac, MD, PhD, [i], Pierre Launay, PhD, [b,d], Giuseppina Caligiuri, MD, PhD, [a,b,j], Antonino Nicoletti, PhD, [a,b], Marie Le Borgne, PhD, [a,b].

Affiliations:

[a] Université Paris Cité and Université Sorbonne Paris Nord, INSERM, LVTS, F-75018 Paris, France.

[b] DHU FIRE, Paris, France.

[c] Department of Vascular and Thoracic Surgery, AP-HP, Bichat Hospital, Université Paris Cité, Paris, France.

[d] INSERM UMRS 1149, Centre de Recherche sur l'Inflammation (CRI), Université Paris Cité, Paris, France.

[e] Department for BioMedical Research, University of Bern, Bern, Switzerland.

[f] Department of Biology and CNRS UMR8113, Ecole Normale Supérieure de Paris-Saclay, Saclay, France.

[g] Department of Pathology, AP-HP, Bichat Hospital, Université Paris Cité, Paris, France.

[h] Department of Vascular Surgery, AP-HP, Ambroise Paré University Hospital, Université Paris Cité, Boulogne-Billancourt, France.

[i] Department of Vascular Surgery, AP-HP, Hôpital Européen Georges Pompidou, Université Paris Cité, Paris, France.

[j] Department of Cardiology, AP-HP, Bichat Hospital, Université Paris Cité, Paris, France.

Address for correspondence:

Marie Le Borgne

LVTS INSERM U1148, 46 rue Henri Huchard, 75018 Paris, France

Tel: +33 1 40 25 75 51; fax: +33 1 40 25 86 02; e-mail: marie.le-borgne-moynier@inserm.fr

Abstract

IgE type immunoglobulins and their specific effector cells, mast cells (MCs), are associated with abdominal aortic aneurysm (AAA) progression. In parallel, immunoglobulin-producing B cells, organised in tertiary lymphoid organs (TLOs) within the aortic wall, have also been linked to aneurysmal progression. We aimed at investigating the potential role and mechanism linking local MCs, TLO B cells, and IgE production in aneurysmal progression.

Through histological assays conducted on human surgical samples from AAA patients, we uncovered that activated MCs were enriched at sites of unhealed haematomas, due to subclinical aortic wall fissuring, in close proximity to adventitial IgE+ TLO B cells. Remarkably, *in vitro* the IgEs deriving from these samples enhanced MC production of IL-4, a cytokine which favors IgE class-switching and production by B cells. Finally, the role of MCs in aneurysmal progression was further analysed *in vivo* in ApoE$^{-/-}$ mice subjected to angiotensin II infusion aneurysm model, through MC-specific depletion after the establishment of dissecting aneurysms. MC-specific depletion improved intramural haematoma healing and reduced aneurysmal progression.

Our data suggest that MC located close to aortic wall fissures are activated by adventitial TLO B cell-produced IgEs and participate to their own activation by providing support for further IgE synthesis through IL-4 production. By preventing prompt repair of aortic subclinical fissures, such a runaway MC activation loop could precipitate aneurysmal progression, suggesting that MC-targeting treatments may represent an interesting adjunctive therapy for reducing AAA progression.

Keywords: Abdominal aortic aneurysm, mast cells, IgE antibodies, tertiary lymphoid organs, B lymphocytes, aortic dissection.

Abbreviations

AAA = abdominal aortic aneurysm; AngII = Angiotensin II; ApoE = apolipoprotein E; DT = diphtheria toxin; MC = mast cell; NAA = non-aneurysmal aortas; RMB = red mast cells and basophil; TLO = tertiary lymphoid organ.

Introduction

Arteries are subjected to recurrent mechanical insults which rise from the luminal side of vessels (Caligiuri et al., 2019). Vessels have intrinsic capacities to ensure prompt healing of local injuries and are assisted in this task by resident and recruited inflammatory cells (Dutertre et al., 2014). However, the persistence of vascular inflammation can eventually amplify the arterial damage and lead to severe and life-threatening conditions including coronary artery disease, strokes or abdominal aortic aneurysms (AAAs) (Libby et al., 2018). Promoting arterial healing by targeting inflammation thus constitutes a major challenge in modern medicine.

In this study, we focused on AAA progression. Monitoring AAA enlargement is problematic due to the discontinuous, so-called 'staccato' growth where month-lasting no-growth/healing periods can be succeeded by a sudden enlargement and again a no-growth/healing period (Kurvers et al., 2004). So far, no pharmacological treatments have been identified to reduce or stop AAA expansion and subsequent arterial rupture, which causes up to 200,000 deaths worldwide each year (Sakalihasan et al., 2018). The only therapeutic option when the aneurysm diameter exceeds a certain value (55mm in men, 50mm in women) is aorta surgery. Therefore, deciphering the molecular pathways involved in AAA healing and/or progression is essential to set up pharmacological alternatives.

Chronic immune responses involve adaptive and innate immunity and their relationship. In particular, we and others have observed that chronic immune stimulation in AAAs leads to local tertiary lymphoid organ (TLO) development within the adventitia (Clement et al., 2015; Guedj et al., 2014; Mohanta et al., 2014; Nicoletti et al., 2013). TLOs contain germinal centre B cells corresponding to B cells undergoing differentiation into plasma cells (Clement et al., 2015). We have reported that TLO development is associated with increased levels of antibodies in the adventitia of human AAAs, in particular IgEs (Clement et al., 2015), which are also

involved in chronic inflammation. Notably, increase in IgE blood concentration correlates with the progression of AAAs and other arterial diseases (Guo et al., 2016; Tuleta et al., 2017). These observations raised the possibility that IgEs are produced locally within the arterial wall.

In parallel, triggered by the binding of IgE at their surface, activated mast cells (MCs) release potent proteases, cytokines and vasoactive molecules, such as leukotriene and histamine, directly or indirectly favouring the detersion of the extracellular matrix and a massive loss of the contingent of medial smooth muscle cells, that could eventually lead to aneurysmal expansion (Sun et al., 2007; Sun et al., 2009; Swedenborg et al., 2011). Interestingly, MC number increases in diseased arteries (Kaartinen et al., 1994; Tsuruda et al., 2008). Furthermore, MCs can promote B cell effector functions (Merluzzi et al., 2010). As a consequence, MCs have been surmised to be detrimental in AAAs (Furubayashi et al., 2007; Sun et al., 2007; Sun et al., 2009). Studies aiming at inhibiting MC activation with pemirolast, a histamine H1 antagonist, were inconclusive regarding their effect on AAA reduction (Sillesen et al., 2015). However, pemirolast cannot uncouple IgE-mediated effector processes, which are by far the most potent and specific trigger of MC activation. Hence, to date, the role of MCs in aneurysmal progression remains elusive.

Here, we aimed at investigating the potential mechanism linking MC activity to IgEs and TLO B cell in aneurysmal progression. To do so, we performed histological and *in vitro* assays using human surgical samples from AAA patients. Furthermore, the putative pathogenic role of MCs in aneurysmal growth was evaluated *in vivo*, by inducing MC depletion in Red Mast cell and Basophil (RMB) - ApoE$^{-/-}$ mice subjected to angiotensin II infusion during the phase of aneurysm progression.

Results

IgE producing-TLOs are associated with aneurysmal wall unhealed fissures in patients

Tissue infiltrated IgE were enriched in aneurysmal samples and soluble IgE plasma levels were elevated in AAA patients compared to control non-aneurysmal aortas (NAAs, Figure 1–figure supplement 1). In parallel, TLOs were found in a majority of AAA samples (20 out of 25, Figure 1A) whereas they were absent in all NAA, in agreement with previous findings (Clement et al., 2015; Guedj et al., 2014; Mohanta et al., 2014; Nicoletti et al., 2013). In particular, adventitial TLOs were consistently found in samples from patients with larger aneurysms (Figure 1B), suggesting their higher frequency in these patients. In these adventitial TLOs, the proportion of germinal centre B cells was dramatically increased (Figure 1–figure supplement 2), suggesting that adventitial TLO B cells in large aneurysms are engaged into an Ab-producing program from which diverse Ig isotypes could emerge. Interestingly, we observed a strong staining for IgEs within the TLO "light zone" (where the centrocytes, i.e. B cells differentiating in immunoglobulins-producing cells, are located (Pipi et al., 2018); Figure 1A) in 45% (n=9) of the samples. Altogether these results suggest that germinal centre B cells within adventitial TLOs situated within large AAAs may actively produce IgE immunoglobulins.

Intriguingly, combined histological analysis of Carstair's, Perl's + DAB and Orcein staining revealed the presence of recent or past wall fissuring with haematoma formation in the media in 92% AAA samples (Figure 1C, Figure 1–figure supplement 3, and Table 1). Indeed, 84% of total AAA tissues (n=21) presented an accumulation of red blood cells (Figure 1C), reflecting the recent occurrence of intramural haematomas. Of note, the diameter of the aneurysmal samples was significantly larger than 3 cm, implying a greater tension and mechanical stress, than the one of the non-aneurysmal aortas (diameter < 3 cm) (Sakalihasan et al., 2018) and an

attentive evaluation of pre-surgery tomography angiograms consistently revealed the presence of at least one detectable aneurysmal wall macroscopic fissure, with radiologic contrast penetrating *via* blood disruptions from the aortic lumen to the aortic wall through the intraluminal thrombus, in 78% of patients with intramural haematomas (Figure 1D and Figure 1–figure supplement 3D). In some samples, we were able to observe the entry site of blood from the lumen on AAA histological sections, suggesting that the fissures leading to intramural haematomas were provoked by tears (micro-fissures) initiated from the aorta lumen (Figure 1–figure supplement 4A-B and 4D-E). Unhealed intramural haematomas could also be evidenced as large areas of ferrous iron deposits next to modest red blood cell accumulation in the media (Figure 1–figure supplement 3B) in 8% (n=2) of samples. Importantly, IgE+ TLOs were frequently localized near these intramural haematomas (Figure 2A-C), suggesting that the maturation of B cells towards IgE-producing cells within adventitial TLOs and the occurrence of micro-fissures are linked.

MCs are enriched at sites of aneurysmal wall fissures and IgE-producing TLOs in human AAAs

In parallel, we observed that the adventitia of AAA patients was significantly enriched in MCs compared to the adventitia of NAA organ donors (Figure 2E-F and Figure 2–figure supplement 1), in agreement with previous observations (Tsuruda et al., 2008). Moreover, MCs were often located next to IgE+ TLOs (Figure 2B-C), and extracellular tryptase+ granules reflecting recent MC activation could be observed around these MCs by immunostaining on AAA sections (Figure 2G-H). Indeed, as compared to NAA samples, adventitial MCs in AAA samples were degranulating, as documented by the expression of the degranulation/MC activation marker CD107a analysed by flow cytometry (Figure 2E-F). Strikingly, MCs enriched in AAA tissues

were consistently found at sites of haematomas on AAA sections (Figure 2D and Figure 1–figure supplement 4C and 4F) where their granule enzymes could favour arterial wall rupture. Altogether, these results suggest that MCs and IgE+ TLOs could concur and be linked together with the occurrence of arterial wall injuries and aneurysmal progression.

Soluble molecules from human AAA adventitia induce MC degranulation and IgE-dependent production of IL-4

Given that MCs displayed an activated phenotype only in the adventitia of AAA patients (Figure 2), we assessed the putative presence of MC activation triggers in the conditioned medium prepared from the adventitia of AAA as compared to control NAA tissues. We observed that conditioned medium from AAA adventitias induced more surface expression of the degranulating marker CD63 and more IL-4 mRNA transcription than conditioned medium from NAA adventitia in cultured ROSA human MCs (Figure 3A-B). This is important because the cytokine IL-4 is required to carry out an IgE antibody class switch recombination and hence allow the production of IgE by B cells (Saunders et al., 2019). Therefore, these results point at an unforeseen function of MCs in AAAs, whereby MCs could orientate the local adaptive immune response generated in adventitial TLOs toward IgE production. In turn, the binding of adventitial IgE on their high affinity receptor on MCs could be responsible for triggering MC activation. To directly assess this hypothesis, we pre-incubated the conditioned medium with anti-IgE DARPin® protein bi53_79 (5 μM) before adding it to MCs (Figure 3C-D). DARPin® protein bi53_79 is a soluble molecule that specifically binds to the IgE-Fc portion thereby preventing IgE binding to FcεRI (Eggel et al., 2014). Whereas treatment of conditioned medium with bi53_79 did not prevent MC degranulation (Figure 3C), it decreased IL-4 mRNA production compared to untreated conditioned medium from AAA tissues (Figure 3D). IgEs

contained in the conditioned medium from AAA adventitias therefore emerge as instrumental in promoting MC IL-4 production.

To assess if IL-4 production, MCs, and IgEs are also linked *in vivo*, we measured IgE, tryptase, and IL-4 quantities in the conditioned medium from AAA adventitias. We found a statistically significant positive correlation between the concentration of IgEs and IL-4 ($p<0.001$), as well as between the concentration of IL-4 and tryptase ($p<0.05$, Figure 3E-F). No such correlations were observed in the plasma of paired patients (Figure 3–figure supplement 1). These observations support the existence of a local amplification loop in the adventitia of AAAs involving IL-4 producing MCs and IgE-producing B cells.

MCs aggravates aneurysmal progression in mice

Previous studies have identified MCs as directly involved in provoking arterial damage (Furubayashi et al., 2007; Sun et al., 2007; Sun et al., 2009). Consistently, the presence of medial/adventitial MCs with an activated phenotype was associated to micro-fissures in our human AAA samples, suggesting that MCs could play a role in the aneurysmal remodelling of the aortic wall, upon the occurrence of tissue fissuring. Therefore, we asked whether specific depletion of MCs could prevent the aneurysmal remodelling in $ApoE^{-/-}$ mice subjected to chronic infusion of Angiotensin II (AngII), a well-known mouse model of aortic dissection eventually followed by aneurysmal progression (Saraff et al., 2003). In this setting, pseudoaneurysm of the abdominal aorta starts within 10 days upon the formation of large intramural haematomas due to the occurrence of multiple medial tears originating from the lumen, at the origin of the main side branches (Trachet et al., 2017). In order to conditionally induce specific MC depletion by DT injection after the occurrence of the aortic fissuring, we crossed $ApoE^{-/-}$ mice with RMB mice (ApoE-RMB mice) (Dahdah et al., 2014). ApoE-RMB

mice were subjected to infusion with AngII for 28 days. We injected DT (or PBS as a control) 14 days after the beginning of AngII infusion. Thus, MCs were depleted after the occurrence of the dissection in this model (Saraff et al., 2003), allowing to evaluate the effect of their depletion on the remodelling of the dissected aortas and their potential effect on aneurysmal progression 14 days later (Figure 4A).

Survival was similar in the two groups (Table 2). As anticipated, the proportion of mice presenting an intramural haematoma at day 28 was equivalent in DT-treated mice (44%, n= 8/18) and in the control group (47%, n=7/17). DT injection almost completely depleted MCs from the aortic tissue (Figure 4B-C) and the peritoneal cavity (Figure 4–figure supplement 1).

MC depletion reduced the expansion of the pseudoaneurysm (Figure 4D-F), comprising the size of the intramural haematoma and of the perivascular adventitial cuff (Figure 4–figure supplement 2A-C). Furthermore, on the cross-sections of the dissected aorta segments stained with picrosirius red we observed that the aortic wall of the pseudoaneurysm of DT-treated mice presented an increased density of collagen compared to control mice (Figure 4E and 4G), especially in the adventitial fibrous cuff (Figure 4–figure supplement 2D). Our data therefore show that MC depletion improves the adventitia fibrotic remodelling which is critical for providing an adequate stiffness and strength subsequently constraining the expansion of the haematoma and the reduction of the aneurysmal progression (McGloughlin, 2011).

Discussion

This study reveals the existence of a potential amplification loop involving IgE+ TLO B cells and MCs at site of tissue fissuring, which could constitute an inflection point in AAA evolution, precipitating aneurysmal progression (Figure 5).

To our knowledge, this is the first time IgE+ germinal centre B cells have been reported in TLOs. Indeed, while they appear early in primary immune responses, coinciding with the peak of IL-4 production, IgE+ cells are unable to populate the long-lived B cell compartment, which explains why IgE+ germinal centres are rarely seen in lymphoid organs (He et al., 2013). Our data show that the observed IgE+ TLOs develop close to aortic wall fissures. Strikingly, the proximity of MCs and IgE+ TLOs at site of tissue injury in the wall of progressive aneurysms supports a possible role for these highly reactive inflammatory cells in the progression of the disease and in the maintenance of the pathologic loop, through their production of IL-4 in response to locally produced IgEs, which in turn sustains the IgE+ germinal centre cells in local TLOs. The correlation between IgE and IL-4 concentrations on one side, and IL-4 and tryptase concentrations on the other side strongly supports the putative interrelated activities of MCs and B cells. Furthermore, the ROSA human MC line is activated by purified IgEs only if these are cross-linked by an anti-IgE antibody (Saleh et al., 2014). Importantly, we did not induce such cross-linking with the conditioned medium. The fact that MCs were nonetheless activated in such experimental conditions implies that the IgEs contained in the conditioned medium were likely cross-linked by their cognate antigens. On the contrary, the fact that blood IgEs failed to activate MCs (data not shown) indicates that they were not circulating as immune complexes and hence strongly suggests that the antigen recognised by IgEs might be specifically present in the aneurysmal aorta. Locally produced IgEs may also directly contribute to AAA progression by promoting the senescence of smooth muscle cells (Guo et al., 2019).

Whereas MC IL-4 production was dependent on IgEs present in the conditioned medium from aneurysmal aorta, degranulation was not. This indicates that besides IgEs, other molecules from the adventitia stimulate MCs. Indeed, other classes of immunoglobulins, which are also enriched in aneurysmal aortas (Clement et al., 2015), cytokines, DAMP-containing molecules and inflammatory mediators released by the injured vascular stroma could also trigger MC degranulation. Further studies focusing on the relationship between IgEs and MC activation could lead to novel therapeutic strategies to reduce chronic inflammatory disorders.

Our pre-clinical *in vivo* data directly support a role for MCs in the fate of aneurysmal development of arterial wall subjected to fissuring and formation of an intramural haematoma. Importantly, for reaching this conclusion, we used the ApoE-RMB mouse model in which the depletion of MCs, conditioned by the use of DT, started only after the initial trigger (aortic dissection). Instead, the rodent models previously used to address this question were constitutively defective in MCs (Sun et al., 2007; Swedenborg et al., 2011; Tsuruda et al., 2008), implying that the deficiency of MCs preceded, and possibly biased, the experimental intervention itself. Furthermore, constitutive MC-deficient models such as $Kit^{W/Wv}$ and $Kit^{W\text{-}sh/W\text{-}sh}$ mice display other hematopoietic abnormalities, notably neutrophilia, thrombocytosis, and macrophage defects (Dahdah et al., 2014; Nigrovic et al., 2008) which could be responsible for some of the effects attributed to MCs. In addition, as resident MCs are present in healthy aortas, constitutive MC depletion could impact aorta homeostasis as well as the formation/progression/rupture of AAAs in these models. By triggering MC depletion after the occurrence of dissections in our $ApoE^{-/-}$ RMB mouse model, we were able to specifically tackle the role played by MCs during the healing processes associated with the progression of AAAs in this model. We found that AAAs in MC-depleted animals displayed improved arterial remodelling with an increased collagen content of the aneurysmal wall, supporting an active role for MCs in collagen degradation and expansion of AAA (Abdul-Hussien et al., 2007;

Dobrin et al., 1984). Mechanistically, MC chymase and tryptase could increase collagen degradation by converting collagenases from their inactive to their active form (Swedenborg et al., 2011). MCs could also inhibit the production of collagen by smooth muscle cells (Wang et al., 2001). Hence, MCs could actively contribute to weaken the arterial wall at sites of micro-fissures and favour the iterative expansion of aneurysms, under the biomechanic stress of intraluminal thrombus (Davis et al., 2019; Wilson et al., 2013). Furthermore, the unhealed micro-fissures could allow the accumulation of plasma proteins into the arterial wall, which is associated to AAA growth (Behr Andersen et al., 2018).

Importantly, the experimental setting we used here is similar to the clinical settings of a recently undertaken clinical trial investigating whether pemirolast, a histamine H1 antagonist acting as a MC stabilizer in allergic conditions, could retard the growth of medium-sized AAAs (Sillesen et al., 2015). This trial in which the major end-point was the change in aortic diameter as assessed by ultra-sound imaging, failed to report a significant improvement in the patients receiving the MC inhibitor. Although this study was elegantly designed and performed, it did not however bring a definitive conclusion regarding MC involvement in AAA pathophysiology because i/ the pemirolast treatment failed to decrease the plasma tryptase levels, indicating a critical dosing issue, ii/ the study interval might have been too short, and iii/ contrary to our study, the effect that MC inhibition might have exerted on tissue composition could not be studied in this clinical study. Hence, in light of our results, we believe it would be interesting to re-evaluate the effect of perimolast (and/or other MC-inhibiting drugs) on AAA growth and rupture rate by targeting patients presenting elevated levels of IgEs and focusing on adventitial remodelling. Inhibiting other key steps of the amplification loop, for instance by using anti-IgE antibodies, could be another promising therapeutic strategy for such patients.

Altogether, our data suggest that locally produced IgEs complexed with lesion-specific antigens activate MCs and trigger IL-4 production, which subsequently promote TLO B cell IgE class

switching. The runaway of this self-sustained local loop could drive repetitive MC degranulation and thus constitute an inflection point in AAA evolution, preventing arterial healing and precipitating AAA rupture (Figure 5).

Materials and Methods

Mice

Apolipoprotein E-deficient ($ApoE^{-/-}$) mice (RRID:IMSR_JAX:002052) were crossed to RMB ($B6.Ms4a2^{tm1Mal}$) mice (Dahdah et al., 2014). RMB mice carry an additive transgene containing the promoter of the high affinity IgE receptor β subunit controlling the human diphtheria toxin (DT) receptor and the tomato red fluorescent protein (Dahdah et al., 2014). The heterozygous offspring were then intercrossed to generate homozygous $ApoE^{-/-}$ RMB mice. Mice were maintained on a C57Bl/6J background and fed a regular show diet. Induction of AAAs, histology and flow cytometry were performed as described below. All investigations on mice conformed to the Directive 2010/63/EU of the European Parliament, and review and approval of the study was obtained from the Comité d'Ethique Paris Nord #121 (APAFIS #12027).

Human samples

AAA tissues and blood were obtained from patients undergoing surgery and enrolled in the RESAA protocol (REflet Sanguin de l'évolutivité des Anévrysmes de l'aorte abdominale) (Caligiuri et al., 2006). As expected (Sakalihasan et al., 2018), AAA patients were predominantly men, and presented risk factors such as age, hypertension, hyperlipidaemia and smoking (Table 3). All patients gave written informed consent, and the protocol was approved by the Comité Consultatif de Protection des Personnes dans la Recherche Biomédicale (CCPPRB, Paris-Cochin, approval no. 2095). Our study complies with the Declaration of Helsinki. Control aortas were sampled from dead organ donors with the authorisation of the French Biomedicine Agency (PFS 09-007, Table 4). Depending on their sizes, samples were cut in several pieces that were used to prepare conditioned medium, and/or digested for flow cytometry analysis, and/or fixed in 3.7% paraformaldehyde (PFA) for histological studies, and

stored in the Inserm human CV biobank (BB-0033-00029), included in the European network BBMRI-ERIC.

Histology and immunofluorescence on human samples

PFA-fixed aortic tissues were paraffin-embedded. Four µm-thick sections were deparaffinised in toluene and rehydrated in ethanol. Sections were subjected to Carstair's stain, orcein stain or Perl's + diaminobenzidine (DAB) stain. Alternatively, sections were incubated with retrieval reagent (R&D Systems), then immunostained using antibodies against IgE (goat polyclonal, Vector Laboratories), MC tryptase (rabbit monoclonal, clone EPR8476, abcam; or mouse monoclonal, clone AA1, abcam), CD20 (mouse monoclonal, clone L26, Dako; or goat polyclonal, Thermofisher), CD117 (rabbit polyclonal, Dako), or glycophorin A (rabbit monoclonal, clone EPR8200, abcam). Immunostaining with isotypes were conducted to verify the specificity of the primary antibodies. Overnight incubation at 4°C with primary antibodies were followed by incubation with fluorophore-coupled anti-species antibodies (Jackson Immunoresearch) for one hour at room temperature. References for antibodies are shown in Supplementary File 1. Nuclei were then stained with Hoechst 53542, and slides were mounted with fluorescent mounting medium (ProLong Gold, ThermoFisher). Slides were kept in the dark at 4°C. Blind analysis was performed for the presence of IgE+ TLOs, MCs and haematomas.

Preparation of conditioned medium and immunodetection of soluble molecules

For the preparation of conditioned medium, the adventitia of AAA and control aortas were separated from the media and cut into small pieces (5 mm^3). The samples were then incubated for 24 hours at 37°C in a standardised volume (6 mL/g of tissue) of RPMI 1640 medium (Gibco) supplemented with antibiotics and antimycotics. The conditioned medium was then centrifuged and the supernatant aliquoted and frozen at -80°C until use.

The IL-4 concentration in conditioned medium from adventitial tissues and serum was analysed by CBA (BD biosciences). Bead fluorescence was recorded on a LSRII flow cytometer (BD). Tryptase was quantified by ELISA (USCN). Immunoglobulins were analysed using a bio-plex pro human isotyping assay (Bio-Rad) according to manufacturer instructions. Beads were analysed on a Bioplex-200 analyser (Bio-Rad). IL-4 and Tryptase were analysed on a different set of patients.

ROSA mast cell line

The ROSA$^{KIT\ WT}$ human cell line (RRID:CVCL_5G49) was cultured in the presence of recombinant human SCF (80 ng/mL, R&D Systems), as described previously (Saleh et al., 2014). Cells were stimulated in the presence of conditioned medium from AAA and control adventitia, or PMA (10ng/mL, Sigma-Aldrich) and ionomycin (1µM, Sigma-Aldrich) (hereafter P+I condition) or IgE (2µg/mL, BeckmanCoulter) for 15 minutes followed by anti-IgE antibody (5µg/mL). After 1 hour of stimulation, the expression of CD63 in MCs was analysed by flow cytometry. Alternatively, after 4 hours of stimulation, cells were collected and dry pellets were frozen for gene expression analysis. In some experiments, 5µM DARPin® protein bi53_79 (Eggel et al., 2014) was added to the conditioned medium. Experiment was repeated twice with similar results.

Gene expression analysis

Total RNAs were extracted from ROSA MCs using the PureLink RNA mini kit (Invitrogen), and mRNA reverse transcription was performed using iScript reverse transcriptase (Bio-Rad). Real time quantitative PCR (RT-qPCR) was performed on a CFX 100 thermocycler (Bio-Rad) using the following primers: forward IL-4: GCAGTTCTACAGCCACCAT; reverse IL-4: ACTCTGGTTGGCTTCCTTCA . One nanogram of cDNA from each sample was mixed with forward and reverse primers (300 nM) and SYBR Green master mix (Bio-Rad). The

amplification program was as follows: A first step of initial denaturation at 95°C for 3 minutes, then 40 cycles of 3 steps: denaturation at 95°C 15 seconds, annealing at 57°C for 15 seconds, and a final extension at 72°C for 30 seconds. The data were analysed using the $2^{-\Delta\Delta Ct}$ formulas: the Ct values of IL-4 were normalised to the average Ct values of RPS18 (forward RPS18: GCGGCGGAAAATAGCCTTTG; reverse RPS18: GATCACACGTTCCACCTCATC) and ACTB (forward ACTB: TCCCTGGAGAAGAGCTACG; reverse ACTB: TTTCGTGGATGCCACAGGAC) and non-treated MCs were used as reference.

Ang-II abdominal aortic pseudoaneurysms in mice

Thirty-eight 28-week-old ApoE-RMB males were used for the experiments, as males are more susceptible to develop AAAs after Angiotensin II (AngII) infusion (Manning et al., 2002). AngII (#A9525, 1 mg/kg/day, Sigma-Aldrich, St Louis, Missouri) was continuously infused into the experimental mice via osmotic mini-pumps (Model 2004, Alzet, Charles River Laboratories) that were surgically implanted subcutaneously in the interscapular region under anaesthesia induced by intraperitoneal injection of ketamine (100 mg/kg) and xylazine (20 mg/kg). Surgery was followed by a buprenorphine intraperitoneal injection (0.1 mg/kg) for analgesia. Three mice (8%) died within the first 10 days. Fourteen days after inducing AAAs through AngII infusion (Saraff et al., 2003), mice received two intraperitoneal injection of DT (1µg/ injection, n=18) at a one-day interval (or PBS in the control group, n=17) in order to deplete MCs. Randomization was achievd by having mice from each experimental group in each cage. Mice were sacrificed at day 28 by intracardiac exsanguination under overdose of anaesthesia (intraperitoneal injection of 150 mg/kg ketamine-HCL and 30 mg/kg xylazine). Before the exsanguination, a cell suspension from the peritoneum was obtained by peritoneal lavage with 5 mL of ice-cold PBS. Blood was withdrawn from the right ventricle of the heart and collected in EDTA tubes for blood cell analysis. The heart and aorta were dissected, photographed and mounted on cryomolds for further histomorphological analysis based on

cryosections. The experiment was repeated twice with similar results. Pooled number of mice from both experiments who survived and developed aneurysms in each group are summarized in Table 2.

Of note, in RMB mice, DT induces both MC and basophil depletion. While basophils fully repopulate the blood within 12 days, MCs repopulation of peripheral tissues such as skin or peritoneum is much slower (Dahdah et al., 2014; Ngo Nyekel et al., 2018). Consistently, two weeks after DT administration (Day 28 of AngII infusion), MCs were totally absent from the peritoneal cavity whereas the basophil population was totally replenished in the blood of ApoE-RMB mice (Figure 4–figure supplement 1). DT injection had no effect on blood basophils, peritoneal MCs, and aortic tissue MCs in control ApoE$^{-/-}$ mice (data not shown).

Histology on mouse tissues

MC depletion was analysed on cryosections of mouse aortic roots stained with Toluidine Blue. Images were captured on a Zeiss Axio Observer Z7 inverted microscope, and MCs were counted manually. A detailed blind analysis of pseudoaneurysms was performed for mouse abdominal aortas displaying macroscopic evidence of the occurrence of a pseudeoaneurysm. Cross-cryosections (10 µm) of the aortic segments taken at different levels of the pseudoaneurysms (every 300 µm) were stained for collagen with picrosirius red (Figure 4–figure supplement 2A). Images were acquired under polarised light. The size of the different layers (media, haematoma, adventitial fibrous cap) and the extent of collagen deposition were quantitatively assessed using Image J.

Image acquisition

Images were digitally captured using an AxioObserver epi-fluorescent microscope equipped with a Colibri 7 LED generator (Zeiss) and an ApoTome system and running Zen Software

(Zeiss). Macroscopic images of the human samples were acquired using the NanoZoomer Digital slide scanner (Hamamatsu Photonics).

Flow cytometry analysis

Mouse blood samples collected in EDTA were incubated in Ammonium-Chloride-Potassium lysis buffer for 5 minutes at room temperature to lyse red blood cells. Cells from blood samples or 1 mL of peritoneal lavage were stained for dead cells with Live/Dead fixable far red Dead cell stain kit (Invitrogen) for 30 minutes at 4°C, then incubated with a purified rat anti-mouse CD16/32 (FcBlock, BD Biosciences) for 15 minutes at 4°C. Cells were then incubated for 20 minutes at 4°C with the following antibodies (from BD Biosciences unless stated otherwise): BV605 rat anti-mouse CD19 (clone 1D3), FITC rat anti-mouse CD117 (clone 2B8), PerCP rat anti-mouse CD45 (clone 30-F11), APC hamster anti-mouse FcεRIα (clone MAR-1, Biolegend), AF700 rat anti-mouse CD3 (clone 172A). References for antibodies are shown in Supplementary File 1.

For human tissue analysis, fresh adventitial layer samples were weighed, cut into small pieces (<1 mm) and digested using a previously described protocol (Fletcher et al., 2011). After a wash step, the cells were stained for dead cells with Live/Dead fixable far red Dead cell stain kit (Invitrogen) for 30 minutes at 4°C, then incubated for 20 minutes at 4°C with a combination of the following mouse anti-human antibodies: AF488 anti-CD3 (clone UCHT1, BD Biosciences), PE anti-CD203c (clone NP4D6, Biolegend), PerCP anti-FcεRIα (clone AER-37, Biolegend), BV421 anti-CD117 (clone 104D2, BD Biosciences), BV500 anti-CD45 (clone HI30, BD Biosciences), PE-Cy7 anti-CD63 (clone H5C6, BD Biosciences), AF700 anti-CD19 (clone HIB19, BD Biosciences), AF647 anti-CD107a (clone H4A3, BD Biosciences), BV421 anti-CD27 (clone O323, Biolegend), BV570 anti-HLA-DR (clone L243, Biolegend), BV785 anti-CD19 (clone HIB19, Biolegend), APC anti-IgD (clone IA6-2, BD Biosciences), FITC anti-

CD38 (clone HIT2, BD Biosciences), PE anti-CD45 (clone HI30, BD Biosciences), BV605 anti-CD45 (clone HI30, BD Biosciences).

For mouse peritoneal cells and human adventitial cells, flow-count fluorospheres (Beckman Coulter) were added to the samples before the acquisition on the cytometer in order to calculate absolute count of cells. Data were acquired on a LSRII flow cytometer or an ARIA III cell sorter (BD Biosciences) and analysed using FACSDiva (BD Biosciences) and FlowJo (TreeStar) softwares.

Statistical analysis

Statistical analysis was performed using the JMP9 and Prism software. To compare two populations, we used Student t-tests or non-parametric Mann-Whitney tests when sample size was too small ($n<10$) or when values were not normally distributed. Paired values were compared using Wilcoxon matched-pairs signed rank test. Pearson correlation coefficients or p-values of chi-square contingency tests were calculated to assess correlation between continuous or categorical variables, respectively. Quantitative data are expressed as mean +/- standard error. Source data with summary statistics can be found in source data files associated to each figure.

Acknowledgments

The authors thank Melanie Gettings for her help with manuscript editing, and Emilie Monnet for her help with the animals.

Sources of funding

This work was supported by the Institut National de la Santé et de la Recherche Médicale (INSERM), the Université Paris Cité, and an Emergence grant from the Département Hospitalo-Universitaire 'Fibrosis, Inflammation, REmodeling in cardiovascular, respiratory and renal diseases' (DHU FIRE, Paris, France). AL was supported by the Domaine d'Intérêt Majeur 'Maladies Cardiovasculaires, Obésité, Rein, Diabète' (CORDDIM) from the Region Ile de France, and the Groupe de Réflexion sur la Recherche Cardiovasculaire (GRRC)/Fédération Française de Cardiologie (FFC, Paris, France).

Related interests

A Eggel is a cofounder and scientific advisor of Excellergy, INC. and ATANIS Biotech AG. M. Arock is on DSMB for AB Science and advisory board for Blueprint Medicines; receives consulting fees and/or honoraries from AB Science, Blueprint Nedicines and Novartis; and declares patent #WO2013064639A1 'Human mastocyte lines, preparation and uses. P Launay is the CEO of Inatherys. Details can be found in ICMJE forms.

Materials availability statement

Use of DARPin® protein bi53_79 and RMB mice requires a MTA. Figure 1–source data 1, Figure 2–source data 1, Figure 3–source data 1, and Figure 4–source data 1, contain the numerical data used to generate the figures.

References

Abdul-Hussien, H., Soekhoe, R. G., Weber, E., von der Thusen, J. H., Kleemann, R., Mulder, A., van Bockel, J. H., Hanemaaijer, R., & Lindeman, J. H. (2007). Collagen degradation in the abdominal aneurysm: a conspiracy of matrix metalloproteinase and cysteine collagenases. *Am J Pathol*, *170*(3), 809-817. https://doi.org/10.2353/ajpath.2007.060522

Behr Andersen, C., Lindholt, J. S., Urbonavicius, S., Halekoh, U., Jensen, P. S., Stubbe, J., Rasmussen, L. M., & Beck, H. C. (2018). Abdominal Aortic Aneurysms Growth Is Associated With High Concentrations of Plasma Proteins in the Intraluminal Thrombus and Diseased Arterial Tissue. *Arterioscler Thromb Vasc Biol*, *38*(9), 2254-2267. https://doi.org/10.1161/ATVBAHA.117.310126

Caligiuri, G., Levy, B. P., Nicoletti, A., & Michel, J.-B. (2019). Role of Biomechanical Stress in the Pathology of the Aorta. In O. H. Stanger, J. R. Pepper, & L. G. Svensson (Eds.), *Surgical Management of Aortic Pathology: Current Fundamentals for the Clinical Management of Aortic Disease* (pp. 163-180). Springer Vienna. https://doi.org/10.1007/978-3-7091-4874-7_11

Caligiuri, G., Rossignol, P., Julia, P., Groyer, E., Mouradian, D., Urbain, D., Misra, N., Ollivier, V., Sapoval, M., Boutouyrie, P., Kaveri, S. V., Nicoletti, A., & Lafont, A. (2006). Reduced immunoregulatory CD31+ T cells in patients with atherosclerotic abdominal aortic aneurysm. *Arterioscler Thromb Vasc Biol*, *26*(3), 618-623. https://doi.org/10.1161/01.ATV.0000200380.73876.d9

Clement, M., Guedj, K., Andreata, F., Morvan, M., Bey, L., Khallou-Laschet, J., Gaston, A. T., Delbosc, S., Alsac, J. M., Bruneval, P., Deschildre, C., Le Borgne, M., Castier, Y., Kim, H. J., Cantor, H., Michel, J. B., Caligiuri, G., & Nicoletti, A. (2015). Control of the T follicular helper-germinal center B-cell axis by CD8(+) regulatory T cells limits atherosclerosis and

tertiary lymphoid organ development. *Circulation*, *131*(6), 560-570. https://doi.org/10.1161/CIRCULATIONAHA.114.010988

Dahdah, A., Gautier, G., Attout, T., Fiore, F., Lebourdais, E., Msallam, R., Daeron, M., Monteiro, R. C., Benhamou, M., Charles, N., Davoust, J., Blank, U., Malissen, B., & Launay, P. (2014). Mast cells aggravate sepsis by inhibiting peritoneal macrophage phagocytosis. *J Clin Invest*, *124*(10), 4577-4589. https://doi.org/10.1172/JCI75212

Davis, F. M., Daugherty, A., & Lu, H. S. (2019). Updates of Recent Aortic Aneurysm Research. *Arterioscler Thromb Vasc Biol*, *39*(3), e83-e90. https://doi.org/10.1161/ATVBAHA.119.312000

Dobrin, P. B., Baker, W. H., & Gley, W. C. (1984). Elastolytic and collagenolytic studies of arteries. Implications for the mechanical properties of aneurysms. *Arch Surg*, *119*(4), 405-409. https://doi.org/10.1001/archsurg.1984.01390160041009

Dutertre, C. A., Clement, M., Morvan, M., Schakel, K., Castier, Y., Alsac, J. M., Michel, J. B., & Nicoletti, A. (2014). Deciphering the stromal and hematopoietic cell network of the adventitia from non-aneurysmal and aneurysmal human aorta. *PLoS One*, *9*(2), e89983. https://doi.org/10.1371/journal.pone.0089983

Eggel, A., Baravalle, G., Hobi, G., Kim, B., Buschor, P., Forrer, P., Shin, J. S., Vogel, M., Stadler, B. M., Dahinden, C. A., & Jardetzky, T. S. (2014). Accelerated dissociation of IgE-FcepsilonRI complexes by disruptive inhibitors actively desensitizes allergic effector cells. *J Allergy Clin Immunol*, *133*(6), 1709-1719 e1708. https://doi.org/10.1016/j.jaci.2014.02.005

Fletcher, A. L., Malhotra, D., Acton, S. E., Lukacs-Kornek, V., Bellemare-Pelletier, A., Curry, M., Armant, M., & Turley, S. J. (2011). Reproducible isolation of lymph node stromal cells reveals site-dependent differences in fibroblastic reticular cells. *Front Immunol*, *2*, 35. https://doi.org/10.3389/fimmu.2011.00035

Furubayashi, K., Takai, S., Jin, D., Muramatsu, M., Ibaraki, T., Nishimoto, M., Fukumoto, H., Katsumata, T., & Miyazaki, M. (2007). The significance of chymase in the progression of abdominal aortic aneurysms in dogs. *Hypertens Res*, *30*(4), 349-357. https://doi.org/10.1291/hypres.30.349

Guedj, K., Khallou-Laschet, J., Clement, M., Morvan, M., Delbosc, S., Gaston, A. T., Andreata, F., Castier, Y., Deschildre, C., Michel, J. B., Caligiuri, G., & Nicoletti, A. (2014). Inflammatory micro-environmental cues of human atherothrombotic arteries confer to vascular smooth muscle cells the capacity to trigger lymphoid neogenesis. *PLoS One*, *9*(12), e116295. https://doi.org/10.1371/journal.pone.0116295

Guo, W., Gao, R., Zhang, W., Ge, W., Ren, M., Li, B., Zhao, H., & Wang, J. (2019). IgE Aggravates the Senescence of Smooth Muscle Cells in Abdominal Aortic Aneurysm by Upregulating LincRNA-p21. *Aging Dis*, *10*(4), 699-710. https://doi.org/10.14336/AD.2018.1128

Guo, X., Yuan, S., Liu, Y., Zeng, Y., Xie, H., Liu, Z., Zhang, S., Fang, Q., Wang, J., & Shen, Z. (2016). Serum IgE levels are associated with coronary artery disease severity. *Atherosclerosis*, *251*, 355-360. https://doi.org/10.1016/j.atherosclerosis.2016.05.020

He, J. S., Meyer-Hermann, M., Xiangying, D., Zuan, L. Y., Jones, L. A., Ramakrishna, L., de Vries, V. C., Dolpady, J., Aina, H., Joseph, S., Narayanan, S., Subramaniam, S., Puthia, M., Wong, G., Xiong, H., Poidinger, M., Urban, J. F., Lafaille, J. J., & Curotto de Lafaille, M. A. (2013). The distinctive germinal center phase of IgE+ B lymphocytes limits their contribution to the classical memory response. *J Exp Med*, *210*(12), 2755-2771. https://doi.org/10.1084/jem.20131539

Kaartinen, M., Penttila, A., & Kovanen, P. T. (1994). Accumulation of activated mast cells in the shoulder region of human coronary atheroma, the predilection site of atheromatous rupture. *Circulation*, *90*(4), 1669-1678. https://doi.org/10.1161/01.cir.90.4.1669

Kurvers, H., Veith, F. J., Lipsitz, E. C., Ohki, T., Gargiulo, N. J., Cayne, N. S., Suggs, W. D., Timaran, C. H., Kwon, G. Y., Rhee, S. J., & Santiago, C. (2004). Discontinuous, staccato growth of abdominal aortic aneurysms. *J Am Coll Surg*, *199*(5), 709-715. https://doi.org/10.1016/j.jamcollsurg.2004.07.031

Libby, P., Loscalzo, J., Ridker, P. M., Farkouh, M. E., Hsue, P. Y., Fuster, V., Hasan, A. A., & Amar, S. (2018). Inflammation, Immunity, and Infection in Atherothrombosis: JACC Review Topic of the Week. *J Am Coll Cardiol*, *72*(17), 2071-2081. https://doi.org/10.1016/j.jacc.2018.08.1043

Manning, M. W., Cassi, L. A., Huang, J., Szilvassy, S. J., & Daugherty, A. (2002). Abdominal aortic aneurysms: fresh insights from a novel animal model of the disease. *Vasc Med*, *7*(1), 45-54. https://doi.org/10.1191/1358863x02vm413ra

McGloughlin, T. M. (2011). Biomechanics and mechanobiology of aneurysms.

Merluzzi, S., Frossi, B., Gri, G., Parusso, S., Tripodo, C., & Pucillo, C. (2010). Mast cells enhance proliferation of B lymphocytes and drive their differentiation toward IgA-secreting plasma cells. *Blood*, *115*(14), 2810-2817. https://doi.org/10.1182/blood-2009-10-250126

Mohanta, S. K., Yin, C., Peng, L., Srikakulapu, P., Bontha, V., Hu, D., Weih, F., Weber, C., Gerdes, N., & Habenicht, A. J. (2014). Artery tertiary lymphoid organs contribute to innate and adaptive immune responses in advanced mouse atherosclerosis. *Circ Res*, *114*(11), 1772-1787. https://doi.org/10.1161/CIRCRESAHA.114.301137

Ngo Nyekel, F., Pacreau, E., Benadda, S., Msallam, R., Abrink, M., Pejler, G., Davoust, J., Benhamou, M., Charles, N., Launay, P., Blank, U., & Gautier, G. (2018). Mast Cell Degranulation Exacerbates Skin Rejection by Enhancing Neutrophil Recruitment. *Front Immunol*, *9*, 2690. https://doi.org/10.3389/fimmu.2018.02690

Nicoletti, A., Khallou-Laschet, J., Guedj, K., Clement, M., Gaston, A. T., Morvan, M., Dutertre, C. A., Michel, J. B., Thaunat, O., & Caligiuri, G. (2013). L19. Lymphoid neogenesis in

vascular chronic inflammation. *Presse Med*, *42*(4 Pt 2), 558-560. https://doi.org/10.1016/j.lpm.2013.01.018

Nigrovic, P. A., Gray, D. H., Jones, T., Hallgren, J., Kuo, F. C., Chaletzky, B., Gurish, M., Mathis, D., Benoist, C., & Lee, D. M. (2008). Genetic inversion in mast cell-deficient (Wsh) mice interrupts corin and manifests as hematopoietic and cardiac aberrancy. *Am J Pathol*, *173*(6), 1693-1701. https://doi.org/10.2353/ajpath.2008.080407

Pipi, E., Nayar, S., Gardner, D. H., Colafrancesco, S., Smith, C., & Barone, F. (2018). Tertiary Lymphoid Structures: Autoimmunity Goes Local. *Front Immunol*, *9*, 1952. https://doi.org/10.3389/fimmu.2018.01952

Sakalihasan, N., Michel, J. B., Katsargyris, A., Kuivaniemi, H., Defraigne, J. O., Nchimi, A., Powell, J. T., Yoshimura, K., & Hultgren, R. (2018). Abdominal aortic aneurysms. *Nat Rev Dis Primers*, *4*(1), 34. https://doi.org/10.1038/s41572-018-0030-7

Saleh, R., Wedeh, G., Herrmann, H., Bibi, S., Cerny-Reiterer, S., Sadovnik, I., Blatt, K., Hadzijusufovic, E., Jeanningros, S., Blanc, C., Legarff-Tavernier, M., Chapiro, E., Nguyen-Khac, F., Subra, F., Bonnemye, P., Dubreuil, P., Desplat, V., Merle-Beral, H., Willmann, M., Rulicke, T., Valent, P., & Arock, M. (2014). A new human mast cell line expressing a functional IgE receptor converts to tumorigenic growth by KIT D816V transfection. *Blood*, *124*(1), 111-120. https://doi.org/10.1182/blood-2013-10-534685

Saraff, K., Babamusta, F., Cassis, L. A., & Daugherty, A. (2003). Aortic dissection precedes formation of aneurysms and atherosclerosis in angiotensin II-infused, apolipoprotein E-deficient mice. *Arterioscler Thromb Vasc Biol*, *23*(9), 1621-1626. https://doi.org/10.1161/01.ATV.0000085631.76095.64

Saunders, S. P., Ma, E. G. M., Aranda, C. J., & Curotto de Lafaille, M. A. (2019). Non-classical B Cell Memory of Allergic IgE Responses. *Front Immunol*, *10*, 715. https://doi.org/10.3389/fimmu.2019.00715

Sillesen, H., Eldrup, N., Hultgren, R., Lindeman, J., Bredahl, K., Thompson, M., Wanhainen, A., Wingren, U., Swedenborg, J., & Investigators, A. T. (2015). Randomized clinical trial of mast cell inhibition in patients with a medium-sized abdominal aortic aneurysm. *Br J Surg*, *102*(10), 1295. https://doi.org/10.1002/bjs.9917

Sun, J., Sukhova, G. K., Yang, M., Wolters, P. J., MacFarlane, L. A., Libby, P., Sun, C., Zhang, Y., Liu, J., Ennis, T. L., Knispel, R., Xiong, W., Thompson, R. W., Baxter, B. T., & Shi, G. P. (2007). Mast cells modulate the pathogenesis of elastase-induced abdominal aortic aneurysms in mice. *J Clin Invest*, *117*(11), 3359-3368. https://doi.org/10.1172/JCI31311

Sun, J., Zhang, J., Lindholt, J. S., Sukhova, G. K., Liu, J., He, A., Abrink, M., Pejler, G., Stevens, R. L., Thompson, R. W., Ennis, T. L., Gurish, M. F., Libby, P., & Shi, G. P. (2009). Critical role of mast cell chymase in mouse abdominal aortic aneurysm formation. *Circulation*, *120*(11), 973-982. https://doi.org/10.1161/CIRCULATIONAHA.109.849679

Swedenborg, J., Mayranpaa, M. I., & Kovanen, P. T. (2011). Mast cells: important players in the orchestrated pathogenesis of abdominal aortic aneurysms. *Arterioscler Thromb Vasc Biol*, *31*(4), 734-740. https://doi.org/10.1161/ATVBAHA.110.213157

Trachet, B., Aslanidou, L., Piersigilli, A., Fraga-Silva, R. A., Sordet-Dessimoz, J., Villanueva-Perez, P., Stampanoni, M. F. M., Stergiopulos, N., & Segers, P. (2017). Angiotensin II infusion into ApoE-/- mice: a model for aortic dissection rather than abdominal aortic aneurysm? *Cardiovasc Res*, *113*(10), 1230-1242. https://doi.org/10.1093/cvr/cvx128

Tsuruda, T., Kato, J., Hatakeyama, K., Kojima, K., Yano, M., Yano, Y., Nakamura, K., Nakamura-Uchiyama, F., Matsushima, Y., Imamura, T., Onitsuka, T., Asada, Y., Nawa, Y., Eto, T., & Kitamura, K. (2008). Adventitial mast cells contribute to pathogenesis in the progression of abdominal aortic aneurysm. *Circ Res*, *102*(11), 1368-1377. https://doi.org/10.1161/CIRCRESAHA.108.173682

Tuleta, I., Skowasch, D., Aurich, F., Eckstein, N., Schueler, R., Pizarro, C., Schahab, N., Nickenig, G., Schaefer, C., & Pingel, S. (2017). Asthma is associated with atherosclerotic artery changes. *PLoS One*, *12*(10), e0186820. https://doi.org/10.1371/journal.pone.0186820

Wang, Y., Shiota, N., Leskinen, M. J., Lindstedt, K. A., & Kovanen, P. T. (2001). Mast cell chymase inhibits smooth muscle cell growth and collagen expression in vitro: transforming growth factor-beta1-dependent and -independent effects. *Arterioscler Thromb Vasc Biol*, *21*(12), 1928-1933. https://doi.org/10.1161/hq1201.100227

Wilson, J. S., Virag, L., Di Achille, P., Karsaj, I., & Humphrey, J. D. (2013). Biochemomechanics of intraluminal thrombus in abdominal aortic aneurysms. *J Biomech Eng*, *135*(2), 021011. https://doi.org/10.1115/1.4023437

Figures

Figure 1. IgE-producing TLOs are present in the adventitia of human AAAs.

(A) Cross-sections of AAAs were stained for CD20 (magenta) and IgE (green). Dense DAPI^{+} lymphoid aggregates highly enriched in CD20+ B cells correspond to TLOs. Several TLOs displayed a strong IgE staining projecting in the CD20+ B cells comprised in the DAPI "light zone" of TLOs (white arrowheads). The magnified inset shows 5 adventitial TLOs (cluster of DAPI+ CD20+ B cells), 3 of which are IgE+. adv: adventitia, m: media, thr; thrombus. Representative image of 9 different samples. Scale bar: 2.5 mm. (B) Maximum diameter size of AAAs depending on the absence (no) or the presence of TLOs. p value (Mann-Whitney test) is indicated on the plots. (C) Serial cross-sections of AAAs were coloured with Carstairs' staining, where fibrin appears in bright red, collagen in blue, red blood cells in yellow and nuclei in black; Perl's+DAB staining allows to visualise redox-active iron; Orcein staining permits to detect elastin fibres. The lumen is at the bottom of each picture and the media (m) is indicated by the blue bar on the side of the pictures. Black arrowheads point at red blood cells outside blood vessels, reminiscent of recent intramural haematomas. Scale bar: 1 mm. Right panels: magnified insets. (D) Contrast-enhanced tomography angiograms of an AAA displaying blood disruption from the aortic lumen to the aortic wall through the intraluminal thrombus (white arrow).

Figure 1–figure supplement 1. IgEs are elevated in the plasma and adventitia of AAA patients.

IgEs were titrated in the plasma (A) and conditioned medium from adventitia (B) of NAA organ donors and AAA patients. Mann-Whitney tests were used to compare groups. **: $p<0.01$; ***: $p < 0.001$.

Figure 1–figure supplement 2. GC B cells and plasma cells are elevated in AAA adventitia.

Adventitia from NAA organ donors and AAA patients were digested and analysed by flow cytometry after the addition of fluorescent count beads. (A) B cells were identified as singlet, autofluorescent$^-$, live CD45$^+$ CD19$^+$ cells, and their number was calculated in each sample, showing a statistically significant increase of B cells in AAA samples. ***, $p < 0.001$, Mann-Whitney test. (B) B cells were identified as in (A), and subsets were defined as follows: naïve B cells, IgD$^+$ CD38$^-$; plasma cells (PC), IgD$^-$ CD38^{hi}; germinal centre B cells (GC), IgD$^-$ CD38$^+$ HLA-DR^{hi}; memory B cells, IgD$^-$ CD38$^-$ HLA-DR$^+$. Representative samples show that GC B cells and plasma cells were present in the adventitia of AAA, while they were barely detected in the matched blood of the AAA patient, or in the adventitia of NAA.

Figure 1–figure supplement 3. AAAs with ancient or no intramural haematomas.

Histological staining of NAAs (A) and AAAs (B-C). Serial sections were stained with Carstairs's stain, Perl's+DAB stain and Orcein stain as in Figure 1C. The squares frame the localisation of the details shown in the insets. The lumen is at the bottom of each picture, and the media (m) is indicated by the blue bar on the side of the pictures. In A, intact elastin fibers

can be seen in the media on the Orcein stain. In B, black arrows indicate iron deposits in the absence of red blood cells, suggestive of an ancient intramural haematoma. An intraluminal thrombus (*) can be seen in C, where no signs of intramural haematoma were seen. Scale bar: 1 mm. (D) Contrast-enhanced tomography angiograms of AAAs. White arrows: blood disruption from the aortic lumen to the aortic wall through the intraluminal thrombus.

Figure 1–figure supplement 4. Proximity of micro-fissures and MC degranulation in human AAAs.

Serial sections of an AAA sample with a micro-fissure (A-C) and from a NAA sample (D-F) were stained with: Carstair's stain (A and D); orcein to reveal elastin fibres (B and E); and tryptase (red) and glycophorin A (gray) to detect MCs/tryptase$^+$ granules and red blood cells, respectively (C and F; the elastin fibres were autofluorescent: green). The pictures in B and C, and E and F, correspond to the green insets in A and D, respectively. The entry site of blood into the aortic wall in the AAA sample can be observed on the Carstair's stain (A, red blood cells appear in yellow). The blood entry site visible on the Carstair's stain (A) and with the glycophorin A stain (C) was associated with degraded elastin fibres (black arrow on orcein stain in B) and the presence of MCs (white arrowhead) and tryptase$^+$ granules (C). Note the normal aspect of the elastin fibers (E) as well as the absence of tryptase and red blood cells (F) in the control. Scale bars: A and D 2.5 mm; others: 200 µm.

Figure 1–source data 1.

This file contains the numerical data and summary statistics used to generate the graphs presented in Figure 1 and its supplements.

Figure 2. IgE-producing TLOs, activated MCs and intramural haematomas are in close proximity in human AAAs.

(A) Cross-sections of AAAs were coloured with Perl's+DAB staining. TLOs (circled with dashed line) are found at proximity of haematomas (arrowheads). Scale bar: 500 µm. (B) Consecutive sections were stained for CD20 (magenta), IgE (green), CD117 (red) and DAPI (grey). B cells ($CD20^+$ and $DAPI^+$) appear in light pink, autofluorescent red blood cells (low intensity in the CD20 channel and $DAPI^-$) appear in magenta, and MCs ($CD117^+$ IgE^+) appear in yellow. Scale bar: 250 µm. (C) Magnified inset highlighting the close proximity of IgE+ TLOs (dashed circle), red blood cells (white arrowheads) and MCs (blue arrows). (D) Magnified inset highlighting MCs (blue arrows) at proximity to intramural haematoma. (E-F) Adventitia from NAA organ donors and AAA patients were digested and analysed by flow cytometry after the addition of fluorescent count beads. Singlet, autofluorescent, live $CD45^+$ cells were selected, and MCs were identified as $CD3^-$ $CD19^-$ $FcεRIa^+$ $CD117^+$ cells (E). The number of MCs (F, left) and activated ($CD107a^{hi}$) MCs (F, right) was calculated in each sample. Error bars represent mean +/- standard error. **, $p < 0.01$; ***, $p < 0.001$, Mann-Whitney test. (G-H) Cross-sections of AAAs were stained for CD20 (magenta), IgE (green), and tryptase (red). MCs ($tryptase^+$ IgE^+) were detected around TLOs. Scale bar: 100 µm. The magnified inset (H) shows a degranulating $tryptase^+$ MC at proximity of a TLO.

Figure 2–figure supplement 1. MCs accumulate in the adventitia of human AAAs.

Carstairs' stain (A) and toluidine blue stain (B-C) on serial sections of a representative micro-fissured AAA sample. MCs appear purple on toluidine blue stain (indicated with black circles). TLOs are circled with a dotted line. Scale bar: 500 µm.

Figure 2–source data 1.

This file contains the numerical data and summary statistics used to generate the graphs presented in Figure 2.

Figure 3. MC degranulation and IgE-dependent IL-4 production in response to conditioned medium from AAA adventitia.

(A-D) ROSA MCs were cultured in the presence of conditioned medium from adventitia of control organ donors (NAA) and AAA patients. DARPin® protein bi53_79 (5 µM) was added (+D) or not (-D) to inhibit IgE binding to MCs' FcεRI (C-D). (A, C) After 1 hr, degranulation (MFI CD63) was assessed by flow cytometry. The dotted line indicates CD63 MFI in non-stimulated cells. (B, D) After 4 hrs, mRNA IL-4 level was analysed by RT-PCR ($2^{-\Delta\Delta Ct}$, normalised to RP18S and non-stimulated cells). *, $p < 0.05$ (A,B: Mann-Whitney test; C,D: Wilcoxon matched-pairs signed rank test). (E, F) Concentrations of IL-4, tryptase, and IgE were measured in conditioned medium from AAA adventitia. *, $p < 0.05$; ***, $p < 0.001$ (Pearson correlation analysis).

Figure 3–figure supplement 1. No correlation between tryptase, IgE and IL-4 in the plasma of AAA patients.

IL-4, tryptase, and IgE concentrations were measured in the serum of AAA patients (same patients as in Fig. 4D). r^2 and p-values from Pearson correlation analysis are indicated.

Figure 3–source data 1.

This file contains the numerical data and summary statistics used to generate the graphs presented in Figure 3 and its supplement.

Figure 4. MCs depletion decreases aneurysmal growth after dissections in ApoE-RMB mice.

(A) Experimental protocol, showing the normal course of pseudoaneurysm development in the Ang II infusion model, and the presence or absence of MCs depending on the treatment (PBS in blue or DT in red). (B) Toluidine blue stain on aortic root cross-sections of DT- and PBS-treated mice. The arrow points to one of the MCs detected in the aortic root adventitia of a PBS control mouse. Scale bar: 250 µm. (C). Quantification of MCs in aortic roots. ***, $p < 0.001$, Mann-Whitney test. (D) Macroscopic images of the hearts and aortas of DT- and PBS-treated mice displaying aneurysms (indicated by arrows). (E) Consecutive cross-sections stained with Masson Trichrome (top, scale bar: 500 µm) or with Sirius red (bottom; polarised light). Aorta outer diameter (F) and collagen density of the aortic wall (G) for mice presenting pseudoaneurysms (PBS: n=7; DT; n=6) were calculated by computer-assisted morphometry on cross-sections stained with Sirius red. Data from sections taken at different levels (every 300 µm) from each pseudoaneurysm were used for calculations (Supplemental Figure 8A), and aligned to the layer with the largest haematoma. Mean +/- standard error; Mann-Whitney test, **: $p < 0.01$; ***: $p < 0.001$.

Figure 4–figure supplement 1. Repopulation of basophils in the blood and MCs in the peritoneum after DT depletion in ApoE RMB mice.

ApoE-RMB mice were treated as in Figure 4A. At day 14 after DT (n=9) or PBS (n=10) injection (day 28 of Ang II infusion), mice were sacrificed. (A) Blood basophils were identified among singlet cells, as $CD45^+$ $Live/Dead^-$ $CD3^-$ $CD19^-$ $Fc\varepsilon RIa^+$ $Tomato^+$ cells (19). (B) Percentage of basophils within singlet cells, $CD45^+$ $Live/Dead^-$ cells. (C) Peritoneal MCs were identified among singlet cells as $CD45^+$ $Live/Dead^-$ $CD3^-$ $CD19^-$ $Fc\varepsilon RIa^+$ $Tomato^+$ cells

CD117^{+} cells [20]. (D) Number of MCs per peritoneal lavage. ***: p<0.0001, Mann-Whitney test. Data are representative of two experiments.

Figure 4–figure supplement 2. MCs promote pseudoaneurysm expansion after dissection in ApoE-RMB mice.

(A) Sections taken at different levels (every 300 µm) from each pseudoaneurysm were used for analysis. (B) Vascular wall layers were defined by computer-assisted morphometry on Sirius red-stained cross-sections (Figure 4E) of pseudoaneurysm (scale bar: 500 µm). Size (C) and collagen density (D) of the different layers were calculated by computer-assisted morphometry, and plotted relatively to the distance from the layer with the largest haematoma. Mann-Whitney test, **: $p < 0.01$; ***: $p < 0.001$.

Figure 4–source data 1.

This file contains the numerical data and summary statistics used to generate the graphs presented in Figure 4 and its supplements.

Figure 5. Schematic overview of the IgE/MC/B cell self-sustained loop in dissecting AAAs.

Locally produced IgEs (and may be other isotype Igs) complexed with lesion-specific antigens activate MCs. Additional triggers from the arterial wall, such as pro-inflammatory cytokines and DAMPs, may contribute to MC activation/degranulation. Proteases and inflammatory mediators hence released from MCs increase the risk of micro-fissures, and MC-derived IL-4 promotes the synthesis of more IgEs by TLO B cells. These events lead to an amplification loop of the pathology.

Tables

Table 1: Patients' characteristics according to the presence of intramural haematomas.

	None (n=2, 8%)	Ancient (n=2, 8%)	Recent (n=21, 82%)
Age (years)	70 +/- 7	67+/- 1	71 +/- 2
Male (%)	100%	100%	90%
Max. aortic diameter (cm)	63 +/- 3	66 +/- 14	61 +/- 4
Diabetes (%)	0%	0%	7%
Hypertension (%)	100%	100%	87%
Hyperlipidaemia (%)	0%	50%	53%
Smoking (%)	50%	50%	93%

Values are mean +/- SEM or %. Ancient intramural haematomas are characterised by ferrous iron deposits with few red blood cells in the media (Figure 1–figure supplement 3B) and recent intramural haematomas are characterized by abundant red blood cells in the media (Figure 1C).

Table 2: ApoE-RMB survival and pseudoaneurysm occurrence.

	PBS (n = 17)	**DT** (n = 18)	**p-value**
Pseudoaneurysm	n = 7 (47%)	n = 8 (44%)	0.85
Death*	n = 0 (0%†)	n = 2 (25%†)	0.15

*, dead mice presented pseudoaneurysms and died 21 days after the beginning of AngII infusion (7 days after DT treatment). †, % of mice with AAA.

Table 3: Patients'characteristics.

	All (n=57)	Histology (n=25)	FC (n=25)	CM (n=37)
Age (yrs)	68 +/- 2	70 +/- 2	73 +/- 2	68 +/- 2
Male	86%	92%	92%	84%
Aneurysm location				
Suprarenal	2.5%	5%	0%	4%
Juxtarenal	2.5%	5%	0%	0%
Subrenal	59%	58%	83%	57%
Subrenal+iliac	36%	32%	17%	39%
Maximum aortic diameter (cm)	61 +/- 2	61 +/- 3	67 +/- 4	63 +/- 3
Clinical Features				
Diabetes	5%	5%	0%	7%
Hypertension	81%	89%	86%	87%
Hyperlipidaemia	40%	47%	58%	37%
Smoking	83%	84%	86%	80%
Anti-coagulants	15%	17%	27%	15%

Values are mean +/- SEM or %, for all AAA samples, or samples according to processing (some samples were used for several kind of analysis). FC: flow cytometry analysis (MCs and/or B cells); CM: conditioned medium (IgE concentration and/or MC stimulation).

Table 4: NAA healthy donors'characteristics.

	All (n=39)	Histology (n=7)	FC (n=16)	CM (n=24)
Age (yrs)	55 +/- 3	53 +/- 9	55 +/- 5	56 +/- 4
Male	61%	80%	56%	61%
Atherosclerotic lesion				
None	28%	29%	31%	25%
Fatty streak	44%	43%	31%	54%
Fibrolipidic	26%	29%	31%	17%
Intraplaque hemorrhage	3%	0%	6%	4%

Values are mean +/- SEM or %, for all NAA samples, or samples according to processing (some samples were used for several kind of analysis). FC: flow cytometry analysis (MCs and/or B cells); CM: conditioned medium (IgE concentration and/or mast cell stimulation).

Additional files

Supplementary file 1: References for antibodies used in this study.

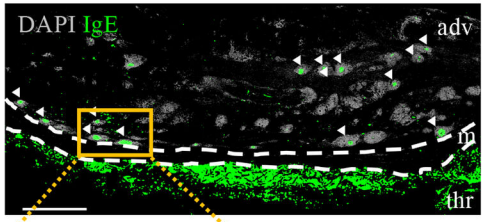
A
DAPI IgE
adv
m
thr

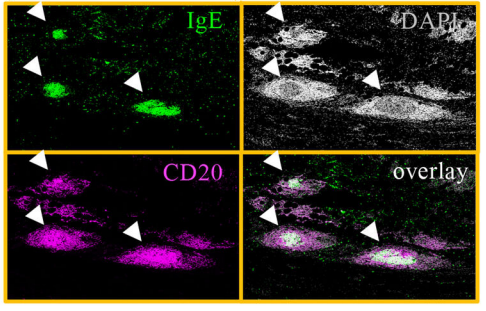
IgE
DAPI
CD20
overlay

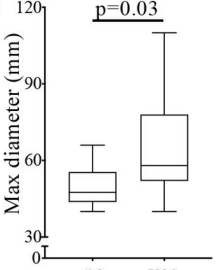
B
p=0.03
Max diameter (mm)
120
90
60
30
0
no
yes
TLO

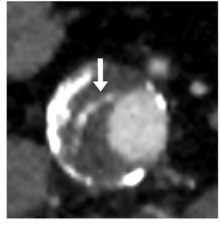
D

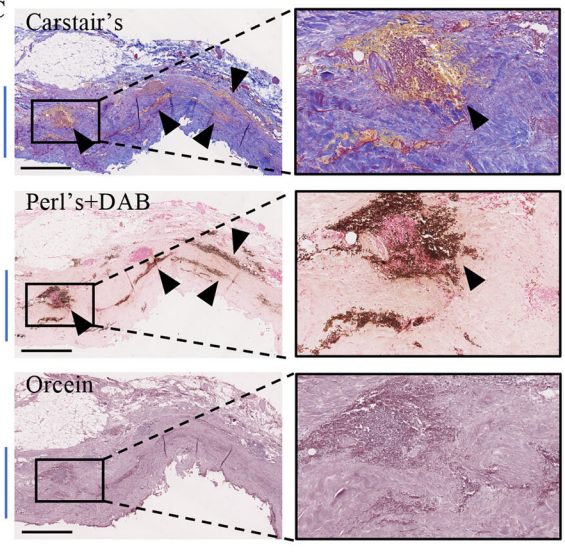
C
Carstair's
Perl's+DAB
Orcein
m
m
m

Figure 1

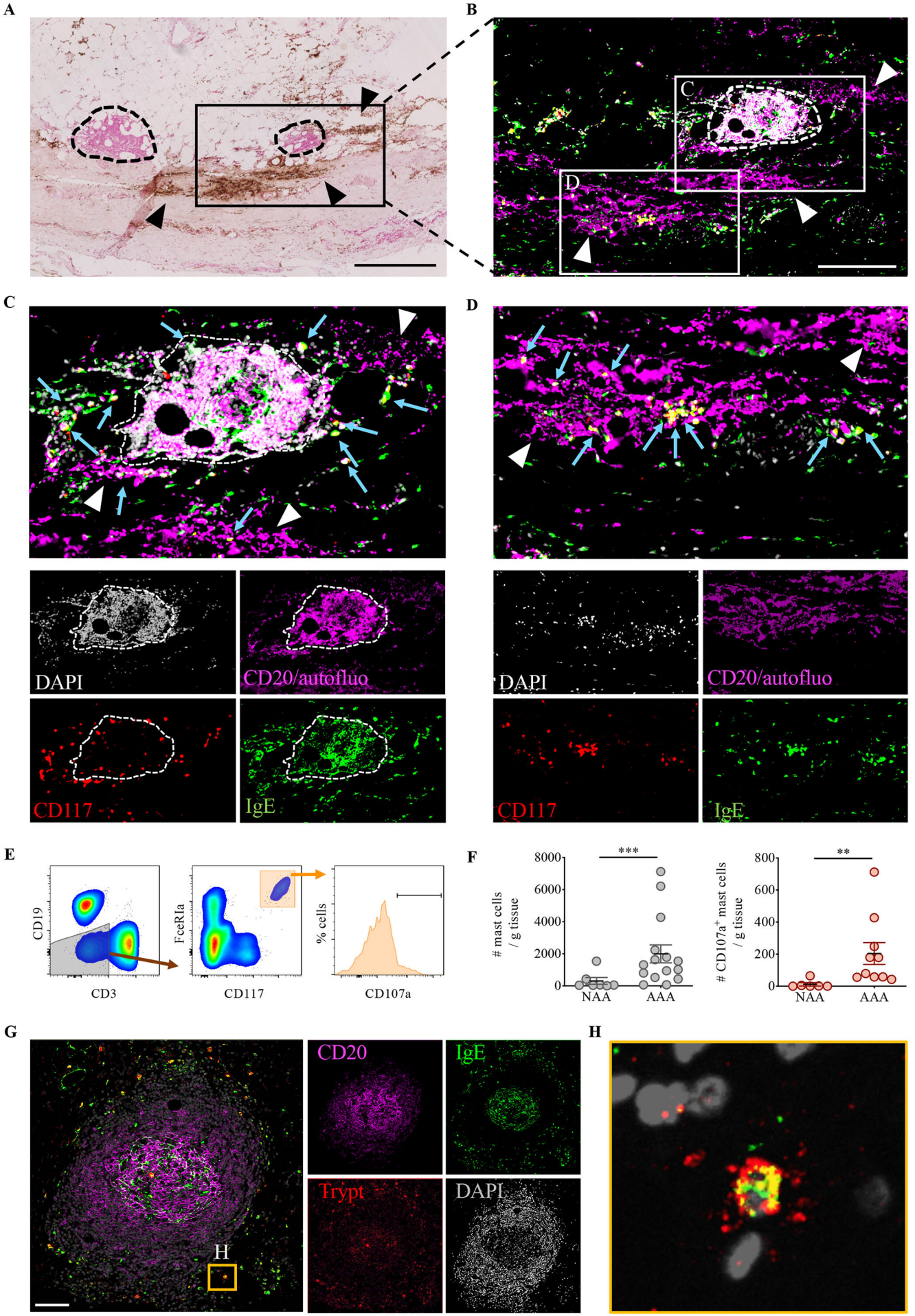
A
B
C
D
DAPI
CD20/autofluo
CD117
IgE
E
CD19
CD3
FceRIa
CD117
% cells
CD107a
F
mast cells / g tissue
8000
6000
4000
2000
0
***
NAA
AAA
CD107a+ mast cells / g tissue
800
600
400
200
0
**
NAA
AAA
G
CD20
IgE
Trypt
DAPI
H
H

Figure 2

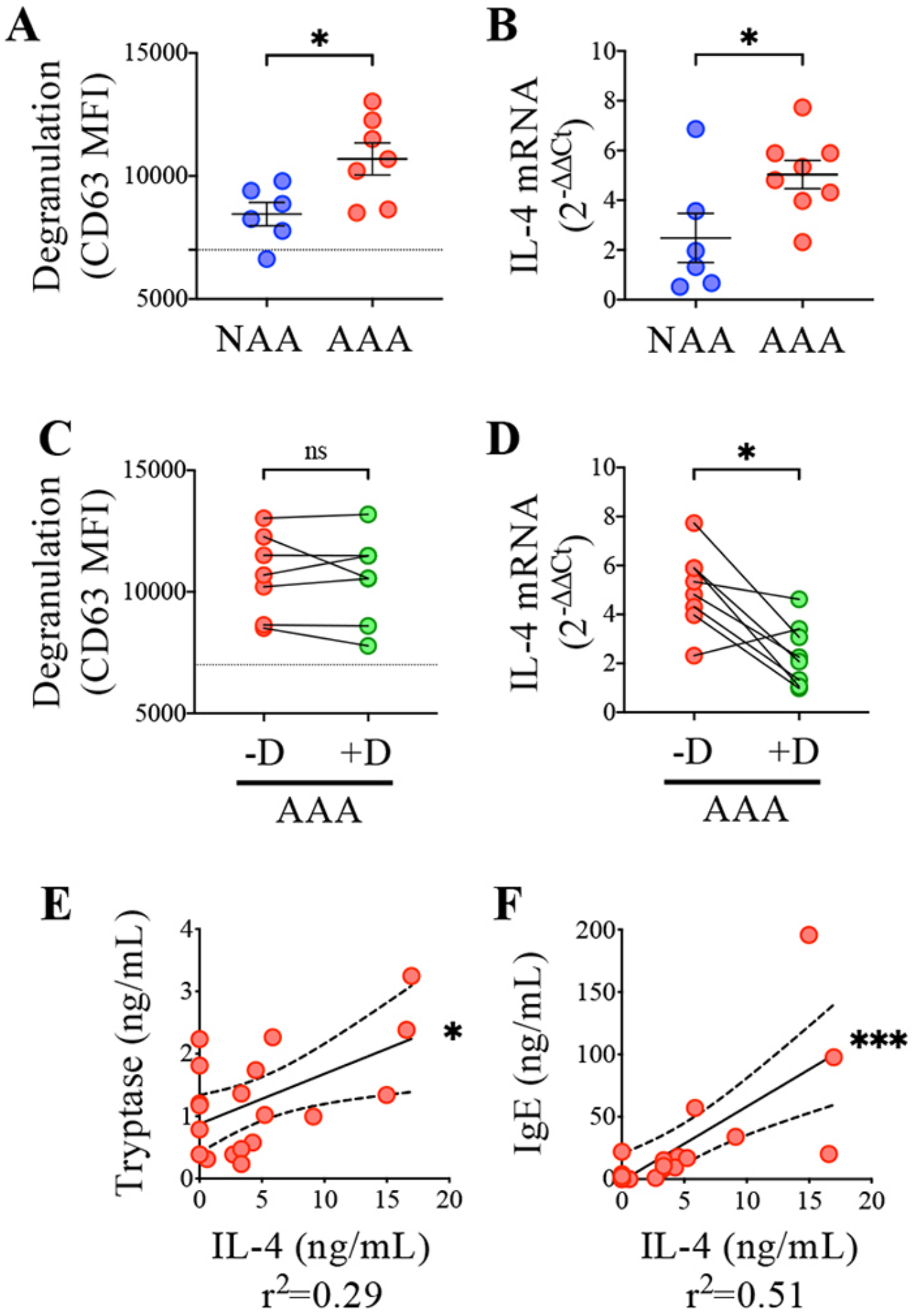
A
Degranulation (CD63 MFI)
15000
10000
5000
*
NAA
AAA
B
IL-4 mRNA (2-ΔΔCt)
10
8
6
4
2
0
*
NAA
AAA
C
Degranulation (CD63 MFI)
15000
10000
5000
ns
-D
+D
AAA
D
IL-4 mRNA (2-ΔΔCt)
10
8
6
4
2
0
*
-D
+D
AAA
E
Tryptase (ng/mL)
4
3
2
1
0
*
0
5
10
15
20
IL-4 (ng/mL)
r2=0.29
F
IgE (ng/mL)
200
150
100
50
0
***
0
5
10
15
20
IL-4 (ng/mL)
r2=0.51

Figure 3

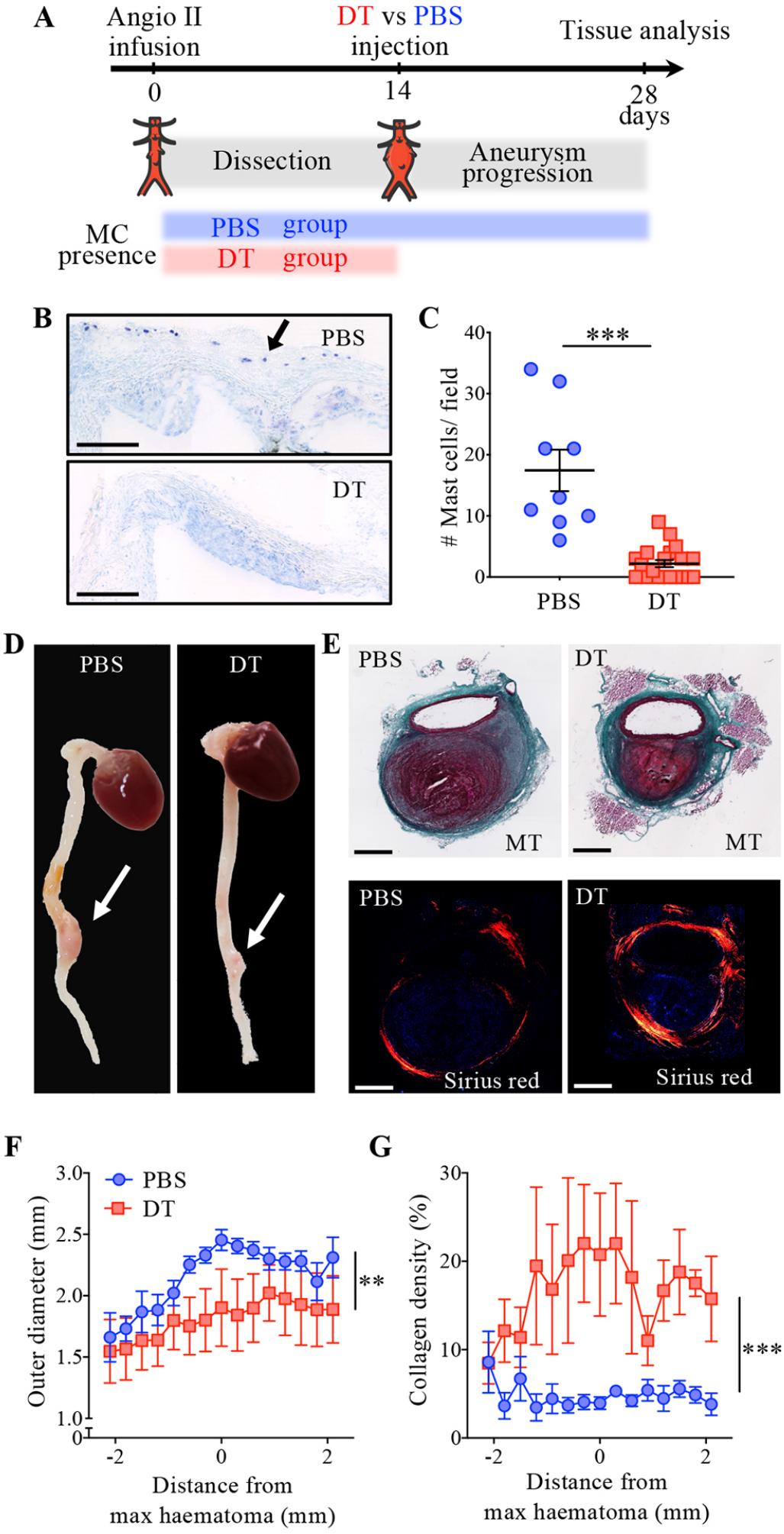
A
Angio II infusion
DT vs PBS injection
Tissue analysis
0
14
28 days
Dissection
Aneurysm progression
MC presence
PBS group
DT group
B
PBS
DT
C
Mast cells/ field
***
PBS
DT
D
PBS
DT
E
PBS
DT
MT
MT
PBS
DT
Sirius red
Sirius red
F
PBS
DT
Outer diameter (mm)
**
Distance from max haematoma (mm)
G
Collagen density (%)
***
Distance from max haematoma (mm)

Figure 4

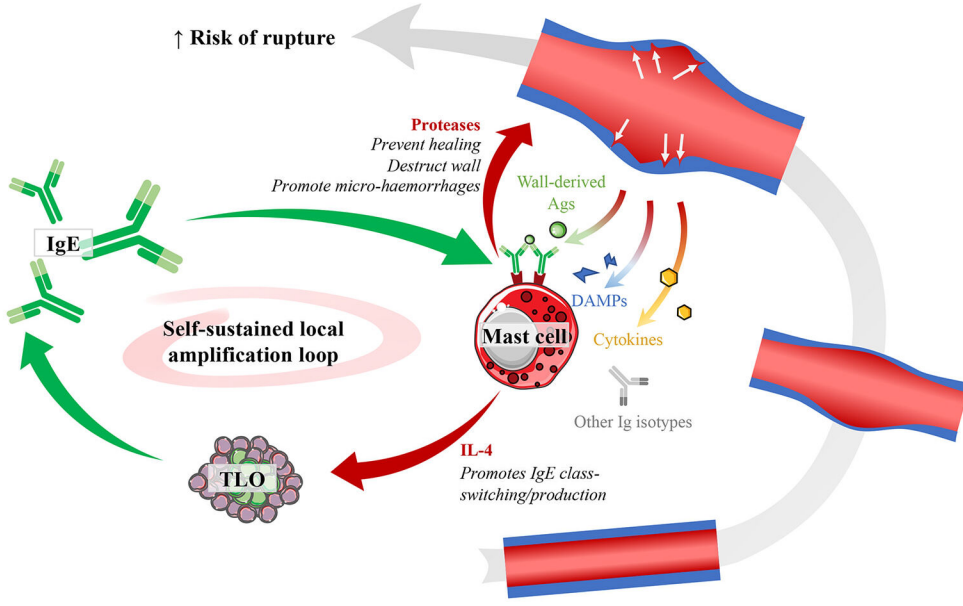
↑ Risk of rupture
Proteases
Prevent healing
Destruct wall
Promote micro-haemorrhages
Wall-derived
Ags
IgE
DAMPs
Mast cell
Cytokines
Self-sustained local
amplification loop
Other Ig isotypes
IL-4
Promotes IgE class-
switching/production
TLO

Figure 5

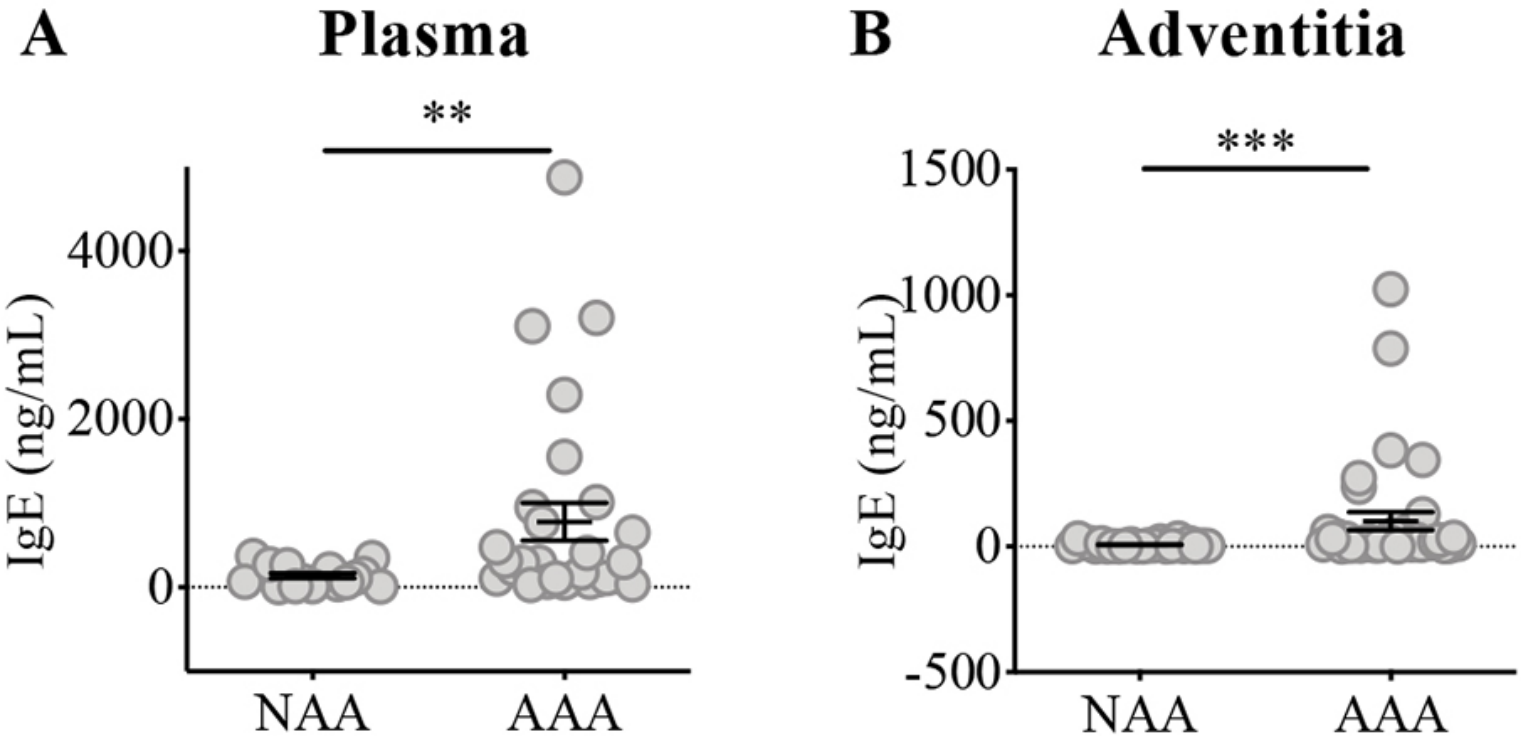

Figure 1-figure supplement 1

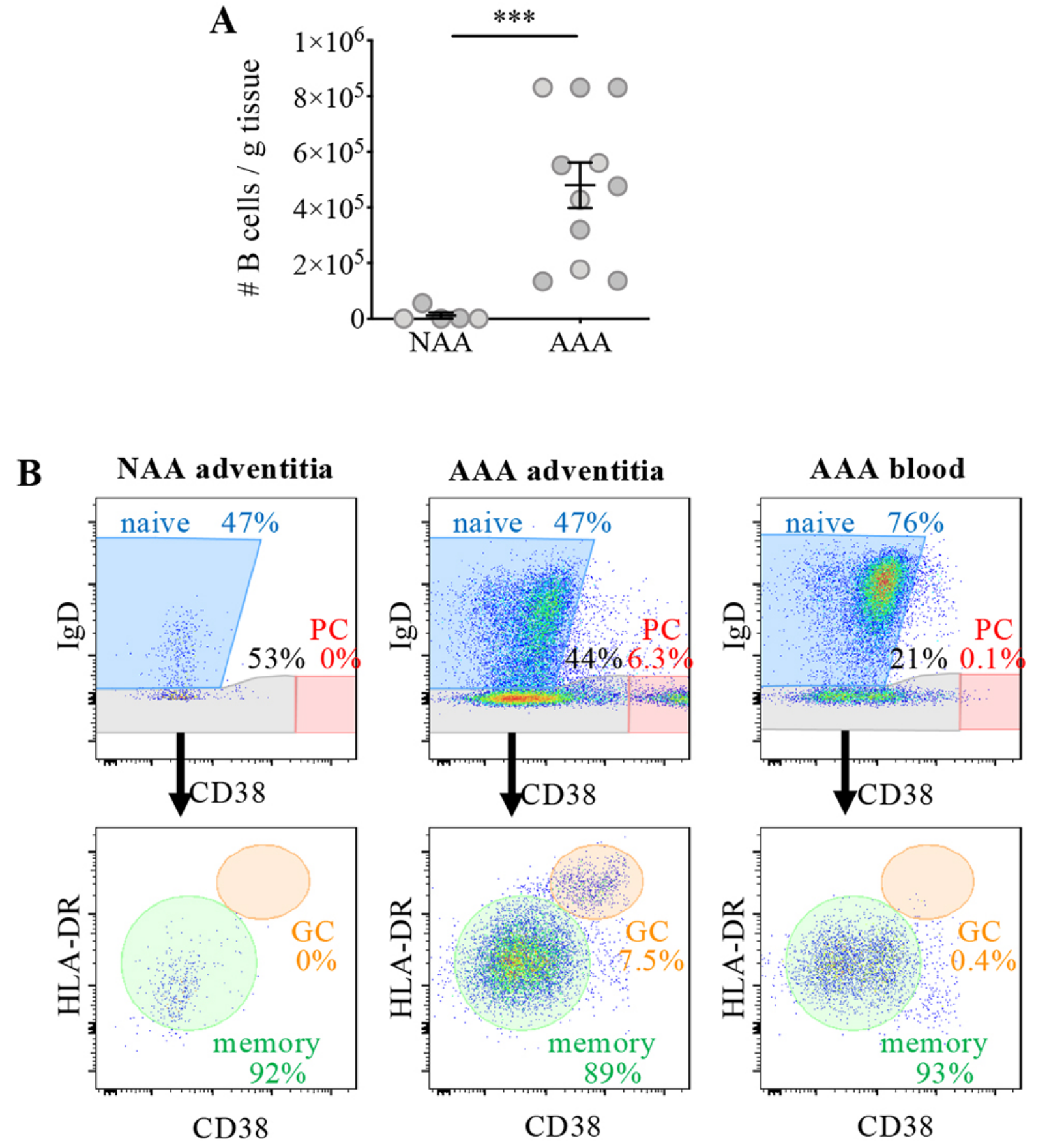

Figure 1-figure supplement 2

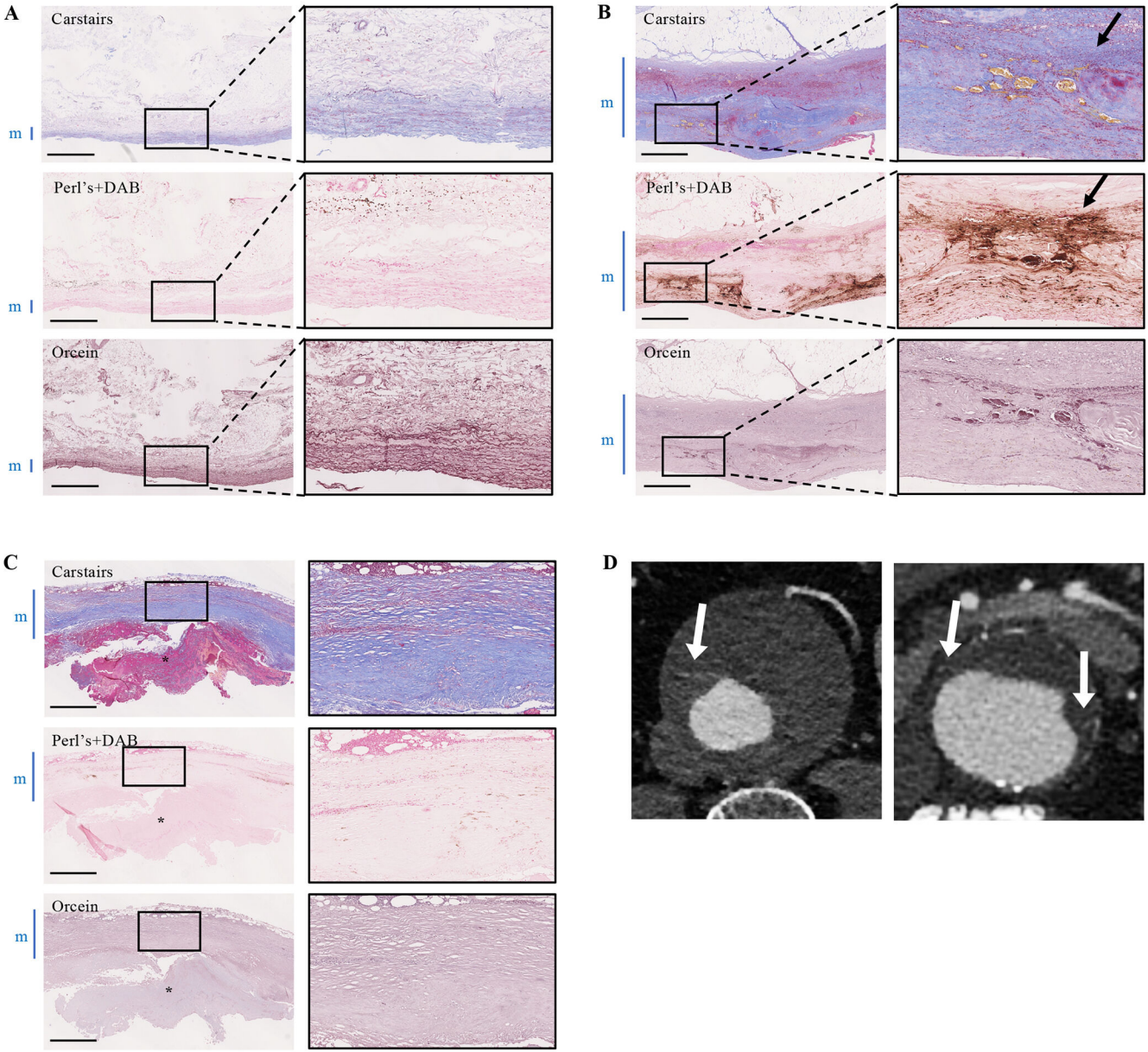

Figure 1-figure supplement 3

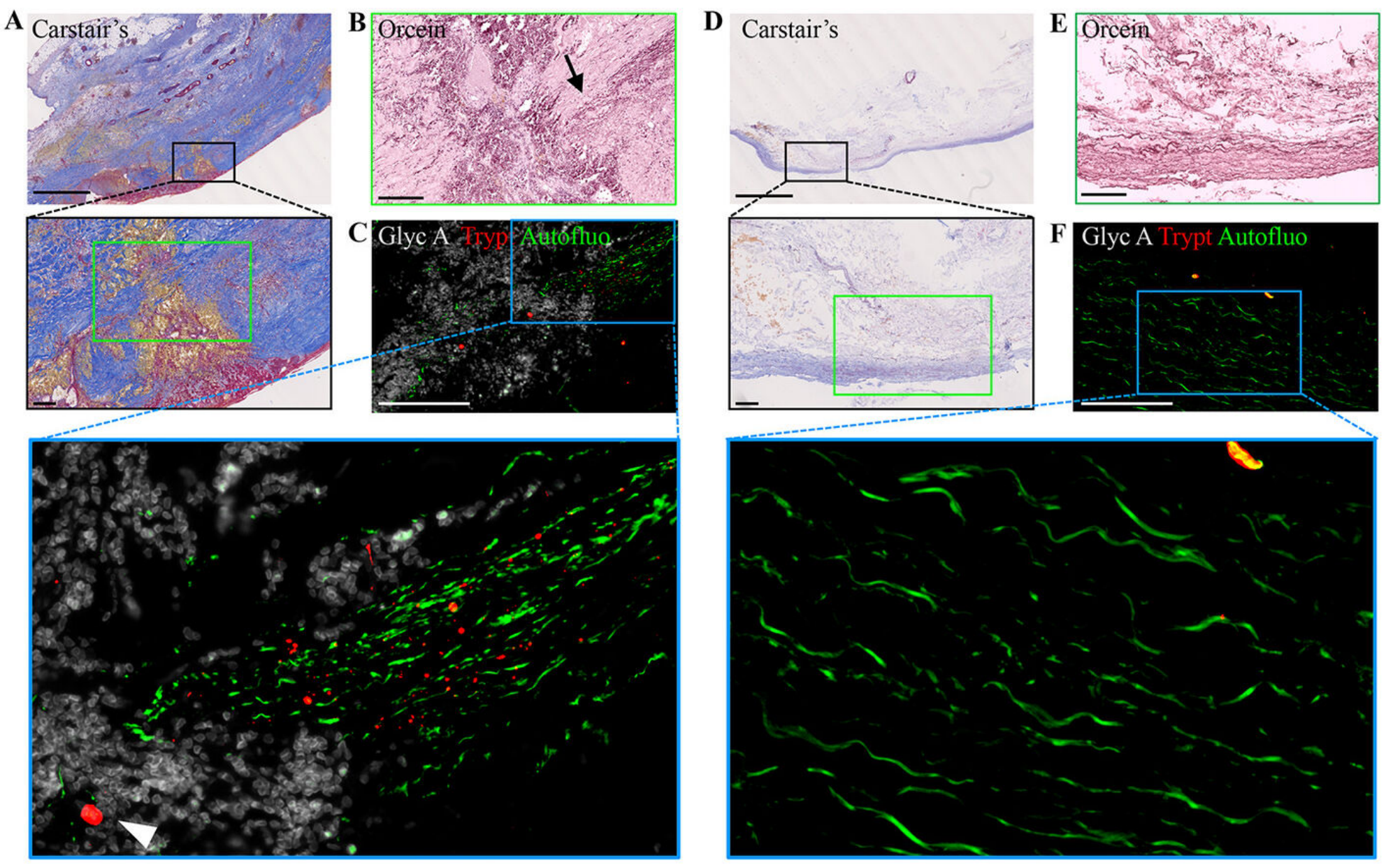

Figure 1-figure supplement 4

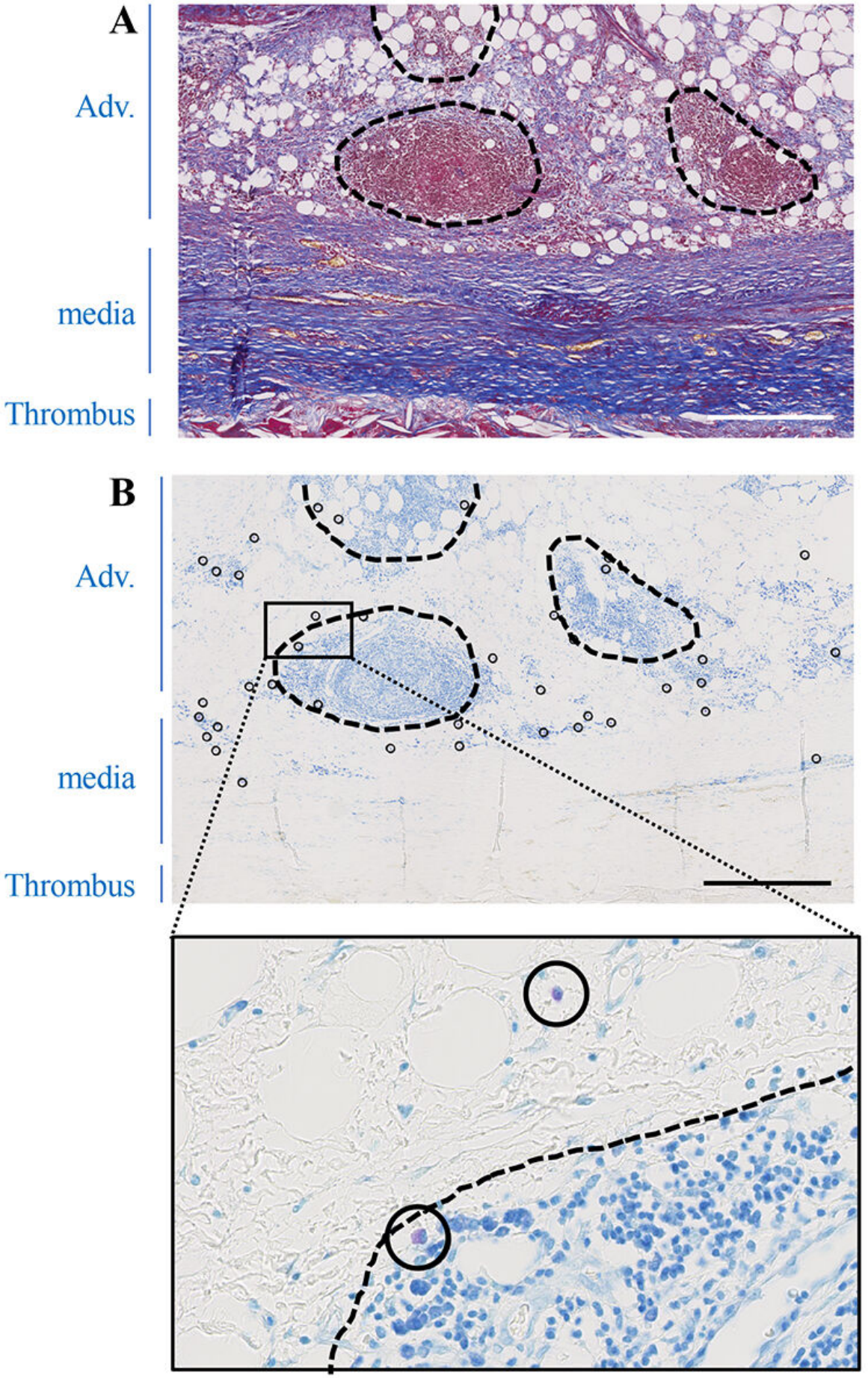

Figure 2-figure supplement 1

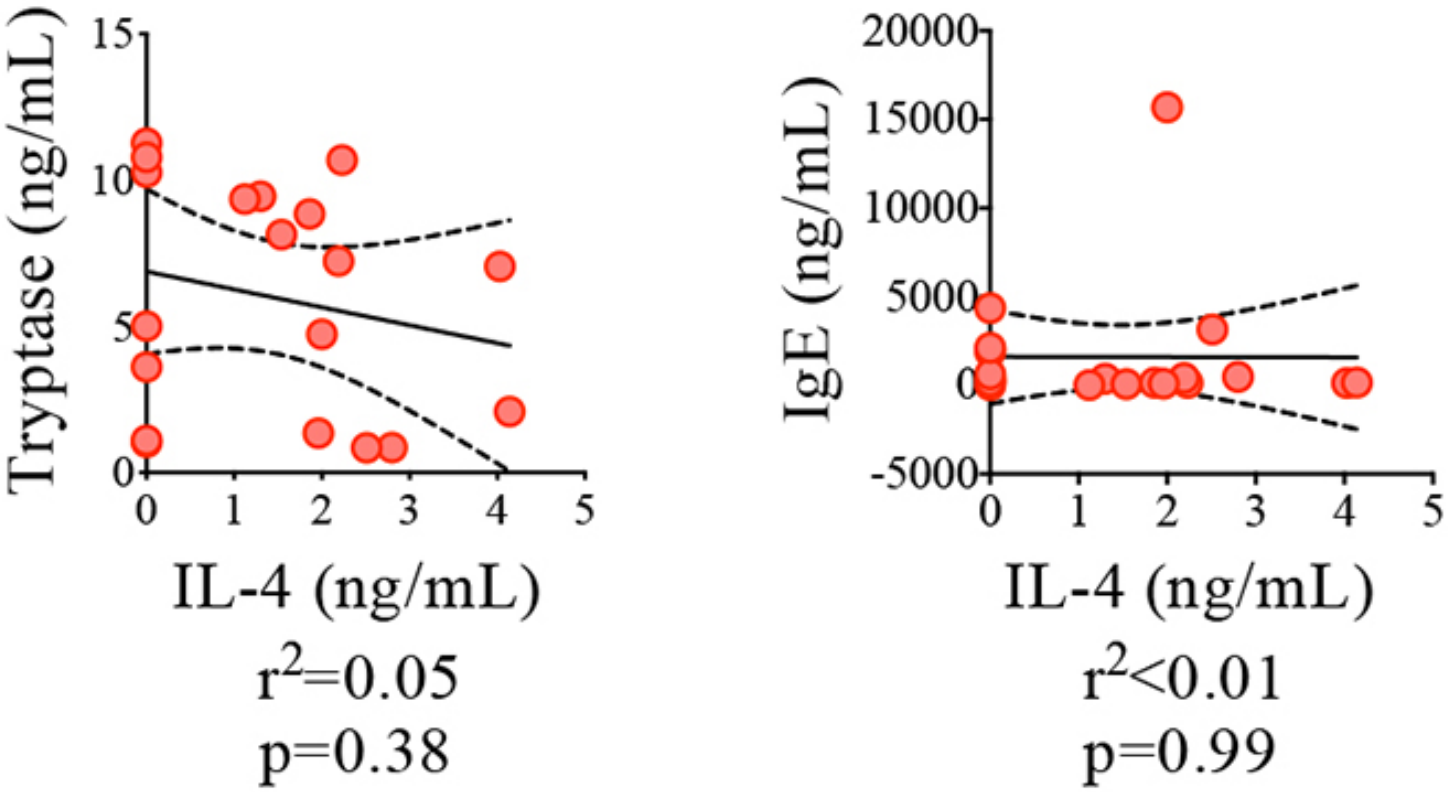

Figure 3-figure supplement 1

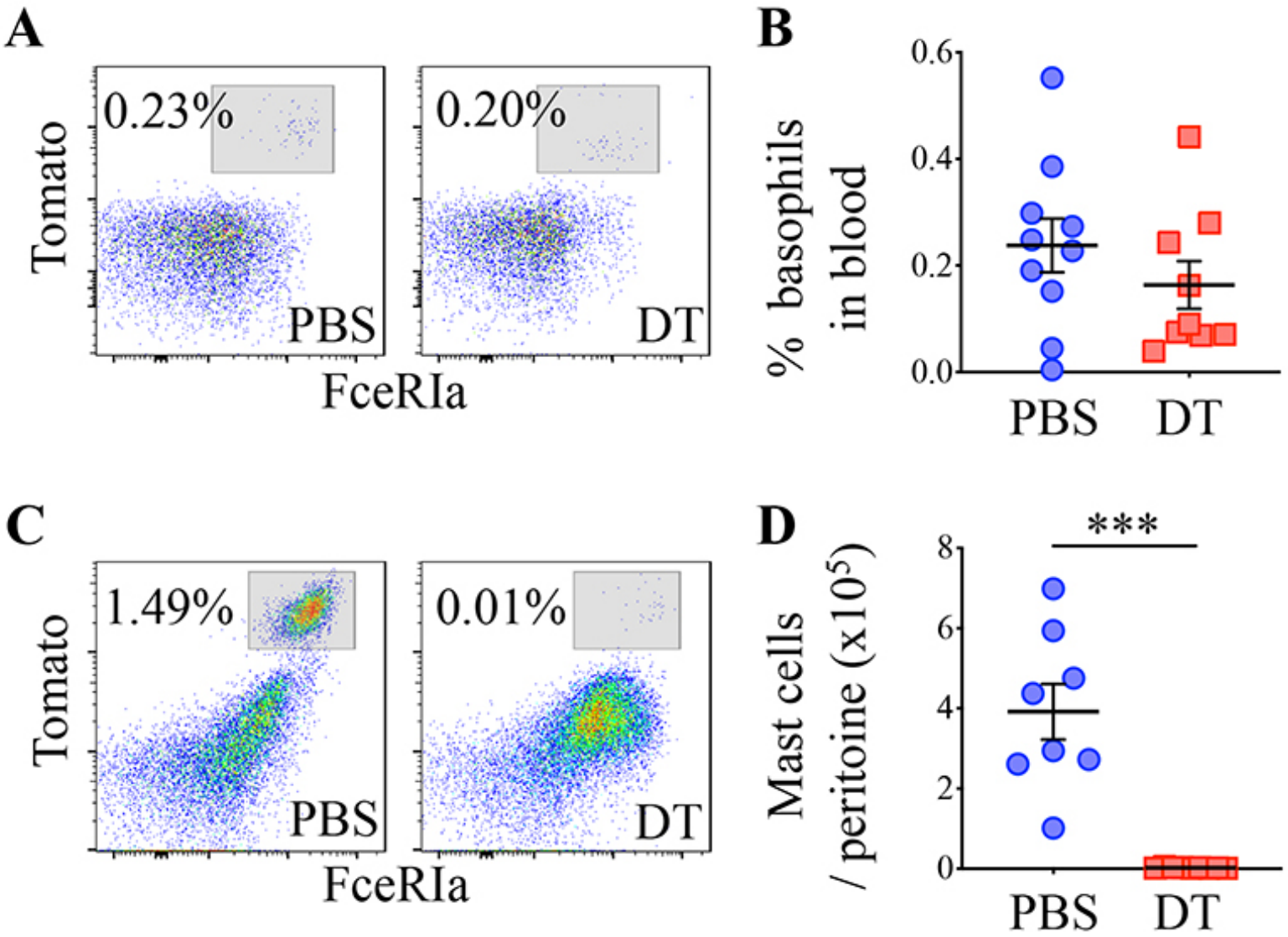

Figure 4-figure supplement 1

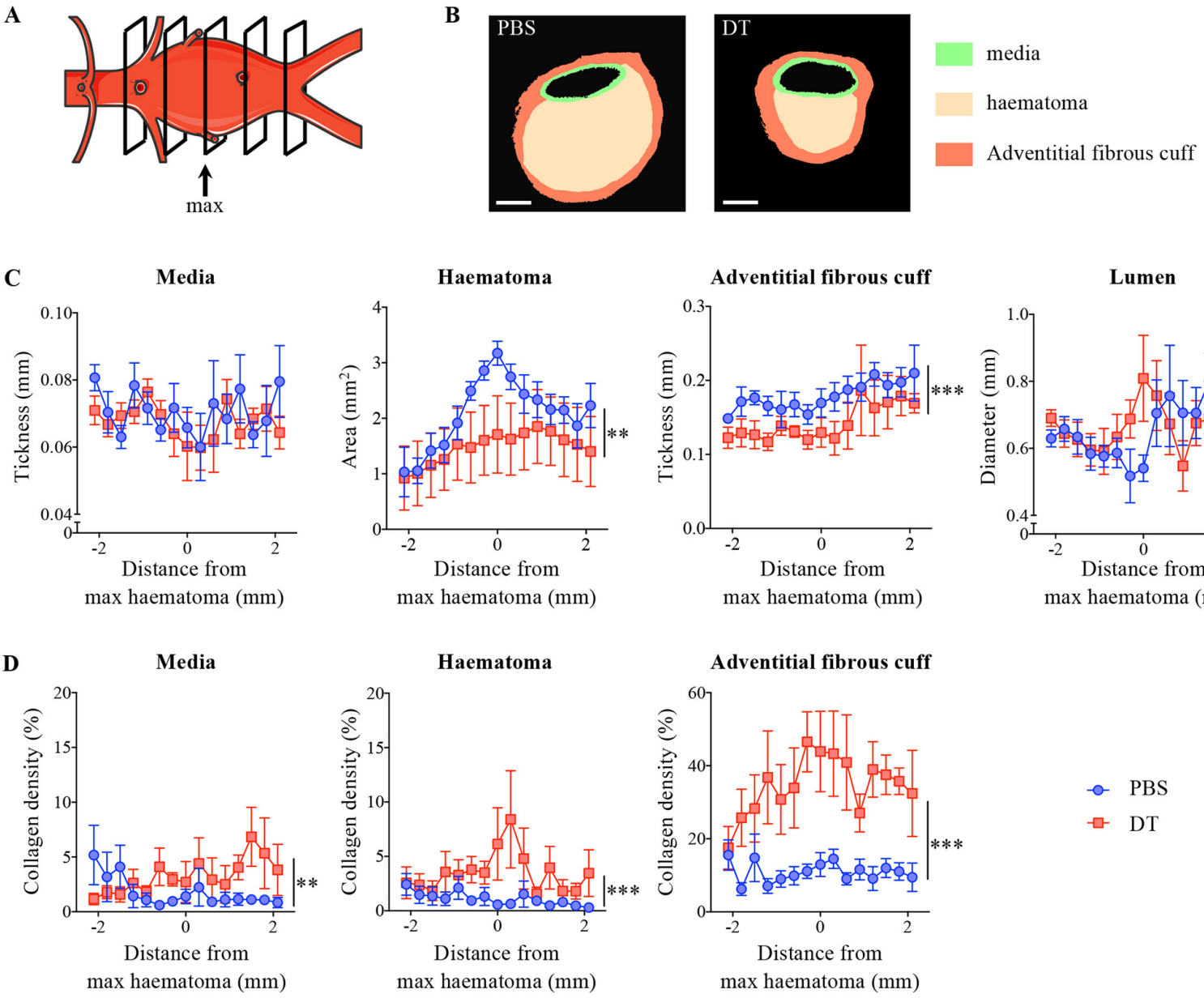

Figure 4-figure supplement 2